**Gaussian Component Decomposition of Pulse Profiles**

| Source | Freq | Comp 1 | | Comp 2/5 | | | Comp 3/6 | | | Comp 4/7 | | |
|---|---|---|---|---|---|---|---|---|---|---|---|---|
| | | Amp | $\sigma$ | Pos | Amp | $\sigma$ | Pos | Amp | $\sigma$ | Pos | Amp | $\sigma$ |
| | MHz | % | ° | ° | % | ° | ° | % | ° | ° | % | ° |
| J0613−0200 | 575 | 100 | 13 | -34 | 40 | 54 | -87 | 19 | 20 | | | |
| | 820 | 100 | 13 | -34 | 77 | 56 | -87 | 33 | 20 | | | |
| | 1410 | 72 | 11 | -35 | 100 | 38 | -76 | 48 | 16 | | | |
| J1012+5309 | 575 | 60 | 11 | -23 | 100 | 46 | -44 | -21 | 7 | 169 | 48 | 27 |
| | | | | 109 | 26 | 4 | 122 | 17 | 7 | -163 | 13 | 10 |
| | 820 | 49 | 11 | -18 | 100 | 45 | -38 | 14 | 8 | 167 | 36 | 26 |
| | | | | 108 | 27 | 4 | 120 | 32 | 14 | | | |
| | 1410 | 86 | 12 | -19 | 100 | 40 | -40 | 13 | 8 | 166 | 24 | 21 |
| | | | | 110 | 41 | 4 | 118 | 39 | 7 | 113 | 18 | 31 |
| J1022+1001 | 575 | 100 | 5 | -12 | 46 | 12 | -18 | 36 | 32 | -4 | 18 | 4 |
| | 820 | 100 | 5 | -11 | 59 | 13 | -22 | 31 | 26 | -3 | 27 | 6 |
| | 1410 | 100 | 5 | -12 | 59 | 9 | -19 | 41 | 24 | -5 | 29 | 4 |
| B1620−26 | 575 | 100 | 14 | -19 | 33 | 21 | 20 | 25 | 14 | | | |
| | 820 | 100 | 14 | -22 | 29 | 24 | 25 | 26 | 20 | | | |
| | 1410 | 100 | 10 | -21 | 22 | 27 | 22 | 21 | 16 | | | |
| J1713+0747 | 575 | 96 | 8 | -5 | 71 | 14 | -22 | 21 | 11 | 45 | 18 | 7 |
| | | | | 8 | 100 | 10 | 19 | 63 | 20 | | | |
| | 820 | 100 | 8 | -6 | 55 | 18 | -27 | 16 | 9 | | | |
| | | | | 9 | 76 | 14 | 22 | 18 | 15 | 33 | 10 | 8 |
| | 1410 | 100 | 8 | -12 | 14 | 11 | -28 | 7 | 9 | 45 | 3 | 8 |
| | | | | 8 | 36 | 10 | 20 | 7 | 15 | | | |
| J1730−2304 | 575 | 30 | 10 | 20 | 100 | 19 | 35 | 32 | 10 | -6 | 23 | 29 |
| | 820 | 31 | 11 | 16 | 100 | 15 | 32 | 60 | 11 | -9 | 34 | 22 |
| | 1410 | 94 | 10 | 15 | 100 | 14 | 31 | 76 | 10 | -9 | 50 | 9 |
| B1821−24 | 575 | 100 | 17 | 108 | 33 | 20 | 177 | 28 | 44 | | | |
| | 820 | 100 | 13 | 106 | 67 | 10 | 177 | 17 | 61 | | | |
| | 1410 | 60 | 9 | 107 | 100 | 6 | -176 | 12 | 18 | 107 | 16 | 45 |
| B1937+21 | 575 | 100 | 13 | -174 | 55 | 13 | 10 | 5 | 8 | -163 | 10 | 8 |
| | 820 | 100 | 9 | -172 | 56 | 11 | 7 | 39 | 4 | -161 | 5 | 3 |
| | 1410 | 100 | 9 | -172 | 45 | 11 | 9 | 38 | 4 | -159 | 6 | 3 |
| J2145−0750 | 575 | 100 | 10 | 69 | 67 | 24 | 79 | 19 | 4 | -60 | 14 | 10 |
| | | | | 7 | 15 | 20 | 32 | 14 | 51 | | | |
| | 820 | 100 | 10 | 70 | 45 | 24 | 78 | 21 | 4 | -59 | 8 | 12 |
| | | | | 10 | 11 | 21 | 33 | 15 | 47 | | | |
| | 1410 | 100 | 9 | 72 | 28 | 26 | 80 | 17 | 4 | | | |
| | | | | 11 | 14 | 21 | 34 | 16 | 35 | | | |

Table 3.1: Gaussian Component Decomposition of Intensity Profiles. A multicomponent Gaussian was fit to the total intensity profile of each source at each frequency. A single component was arbitrarily chosen as the reference (usually the strongest component at some frequency). Column 3 gives the amplitude of this reference component relative to the component with maximum height (%). Column 4 gives the FWHM of the reference component in degrees. The first column of each remaining component gives the phase location in degrees relative to the reference component. The remaining two columns are again amplitudes relative to the maximum component, and FWHM in degrees. For objects which required more than four components, components 5-7 are displayed on a second line. In two cases, one of the components was not required at one of the frequencies, and it has been left blank so as to keep the remainder of the components aligned across frequency.

# Chapter 3

# Polarization Observations of Millisecond Pulsars

## 3.1 Data Presentation

The data discussed in the previous chapter are presented for each pulsar and radio frequency in Figures 3.1-3.34. For each object for which multi-frequency data are available, three figures are presented. For these objects, the total intensity profiles were decomposed into Gaussian components, using fitting software developed elsewhere (Kramer 1994, Kramer *et al.* 1994). The resulting Gaussian components are displayed at a single frequency in the first figure for each pulsar. The results of these fits at all frequencies are presented in Table 3.1. For each pulsar and radio frequency, the relative positions, relative amplitudes, and widths of the Gaussian components are given.

The polarization profiles across the full pulse period for all three observing frequencies are shown in the second figure for each object. This allows examination of the profile and polarization evolution with frequency, and object-to-object comparison of the duty cycles. In each case, the intensity, normalized to a peak value of 1, is plotted as a solid line against pulse phase in degrees. The fractional linear polarization is plotted as a dotted line, while the fractional circular polarization is shown by a dashed line. The polarization position angle (PPA) is displayed in the bottom panel of each plot for values of the linear polarization which exceed the $rms$ away from the pulse by a set threshold $T$. The pulse phase in milliseconds is shown along the top of each plot. The phase and PPA alignment between frequencies is arbitrary. Finally, the polarization properties for a region surrounding the pulsed emission is shown for each pulsar at a single frequency, to clarify the detailed features.

Table 3.2 summarizes the data reduction of the polarization profiles presented in Figures 3.1-3.34. For each source and radio frequency, column 2 indicates the

**Polarization Profile Summary**

| Source | Freq MHz | Epoch yymon | Integration Time (s) | Resolution ($\mu$s) | PPA Thresh | Alignment Technique |
|---|---|---|---|---|---|---|
| B0531+21 | 610 | 96nov/dec | 125100 | 34.1 | 1 | sa-cc[a] |
| J0613−0200 | 575 | 97jul | 16560 | 17.1 | 2 | sa-cc |
| | 820 | 97feb/apr/jul | 51230 | 18.4 | 2 | sa-cc |
| | 1410 | 97apr | 1500 | 18.4 | 2 | add |
| J0751+1807 | 1410 | 97mar | 2609 | 18.2 | 2 | align |
| J1012+5309 | 575 | 97jul | 7920 | 18.3 | 1 | ephem |
| | 820 | 97feb/apr/jul | 47221 | 20.5 | 1 | ae-cc[b] |
| | 1410 | 97mar/97apr | 6200 | 10.3 | 1 | sa-cc |
| J1022+1001 | 575 | 97jul | 7560 | 18.3 | 1 | ephem |
| | 820 | 97feb/apr/jul | 56895 | 27.4 | 1 | ae-cc |
| | 1410 | 97mar/97apr | 5864 | 18.3 | 1 | sa-cc |
| J1518+4904 | 1410 | 97mar | 1818 | 123. | 2 | sa-cc |
| B1620−26 | 575 | 97jul | 27900 | 47.9 | 1 | ephem |
| | 820 | 97feb/apr/jul | 56164 | 34.3 | 1 | sa-cc |
| | 1410 | 97mar/97apr | 6352 | 34.3 | 1 | sa-cc |
| J1640+2224 | 1410 | 97mar/97apr | 1265 | 18.3 | 2 | add |
| J1643+1224 | 1410 | 97mar/97apr | 5104 | 18.3 | 2 | ephem |
| J1713+0747 | 575 | 97jul | 39060 | 13.7 | 1 | ephem |
| | 800 | 95feb | 6000 | 22.9 | 1 | sa-cc |
| | 820 | 97feb/apr/jul | 71168 | 11.4 | 1 | ae-cc |
| | 1410 | 97mar/97apr | 5487 | 2.3 | 3 | ephem |
| J1730−2304 | 575 | 97jul | 12960 | 27.4 | 2 | add |
| | 820 | 97feb/apr/jul | 20398 | 27.4 | 2 | ae-cc |
| | 1410 | 97apr | 1500 | 27.4 | 2 | add |
| B1821−24 | 575 | 97jul | 25380 | 17.1 | 1 | add |
| | 820 | 97feb/apr/jul | 58501 | 12.0 | 1 | sa-cc |
| | 820 | 97feb | 13800 | 24.0 | 1 | add |
| | 820 | 97apr | 31201 | 24.0 | 1 | add |
| | 820 | 97jul | 13501 | 24.0 | 1 | add |
| | 1410 | 97mar/97apr | 3022 | 9.1 | 1 | add |
| B1937+21 | 575 | 97jul | 17161 | 2.0 | 1 | add |
| | 820 | 97feb/apr/jul | 31740 | 1.1 | 3 | ae-cc |
| | 1410 | 97mar/97apr | 3900 | 1.1 | 2 | sa-cc |
| J2145−0750 | 575 | 97jul | 38879 | 54.9 | 3 | ephem |
| | 800 | 95feb | 2400 | 78.6 | 1 | add |
| | 820 | 97apr | 3000 | 32.0 | 3 | add |
| | 1410 | 97apr | 840 | 64.0 | 3 | add |

[a] Sub-average over short times, then align via cross-correlation

[b] Add within an epoch, and align via cross-correlation between them

Table 3.2: Polarization Profile Summary. For each polarization profile displayed in Chapter 3, the observing frequency and epoch are listed in columns two and three. Column 4 displays the accumulated integration time of the displayed profile, with the resolution of the plot in $\mu$s in column 5. The technique used to align the data is in column 6.

epoch(s) at which the displayed observations were taken. The total integration time of the profile is given by column 3, and the plot resolution and PPA threshold $T$ are in columns 4 and 5. Column 6 indicates the alignment technique used to produce the polarization profile.

**Polarization of Millisecond Pulsars**

| Source | Frequency | $\frac{P}{I}$ | $\frac{V}{I}$ |
|---|---|---|---|
| | MHz | % | % |
| J0613-0200 | 575 | 4.7±2.3 | -4.6±3.2 |
| | 820 | 9.1±2.02 | -2.2±2.1 |
| | 1410 | 6.8±3.7 | 4.6±5.6 |
| J1012+5307 | 575 | 36.7±2.4 | 1.5±2.0 |
| | 820 | 41.6±4.0 | 5.6±3.5 |
| | 1410 | 37.1±1.1 | -3.6±1.7 |
| J1022+1001 | 575 | 56.9±0.4 | -13.3±0.4 |
| | 820 | 41.0±1.2 | -12.2±1.4 |
| | 1410 | 44.3±0.4 | -14.2±0.5 |
| B1620-26 | 575 | 16.2±2.3 | -13.5±3.7 |
| | 820 | 24.3±1.2 | -9.5±1.5 |
| | 1410 | 28.2±1.2 | -15.2±1.9 |
| J1713+0747 | 575 | 21.1±0.9 | -5.7±1.1 |
| | 820 | 14.5±1.1 | -2.3±1.5 |
| | 1410 | 18.1±0.3 | -0.68±0.5 |
| J1730-2304 | 575 | 4.7±1.5 | -3.8±2.0 |
| | 820 | 9.3±1.5 | -23.1±2.6 |
| | 1410 | 19.1±1.3 | -25.4±2.0 |
| B1821-24 | 575 | 40.4±4.5 | -5.1±5.1 |
| | 820 | 36.9±4.0 | 10.0±4.6 |
| | 1410 | 36.2±8.5 | -6.9±8.5 |
| B1937+21 MP | 575 | 57.9±0.3 | -2.1±0.4 |
| | 820 | 47.5±0.2 | 3.1±0.2 |
| | 1410 | 30.0±0.2 | 0.5±0.3 |
| B1937+21 IP | 575 | 10.1±0.4 | -1.7±0.7 |
| | 820 | 8.8±0.3 | 3.8±0.4 |
| | 1410 | 13.1±0.5 | 1.6±0.7 |
| J2145-0750 | 575 | 9.8±0.7 | 3.2±1.1 |
| | 820 | 8.8±0.6 | 7.8±0.8 |
| | 1410 | -1.0±1.2 | -0.53±2.2 |

Table 3.3: Polarization of Millisecond Pulsars. For each pulsar and observing frequency (columns 1 and 2), the fractions of the radiation in linear and circular polarizations, averaged across the pulse, are displayed in columns 3 and 4. The quoted errors are based on the *rms* of the profile, and do not include systematic calibration errors.

The total fraction of polarization across the pulse profile was calculated for the multi-frequency data. Table 3.3 contains the total linear and circular polarizations in columns 3 and 4.

## 3.2 PSR J0613−0200

This 3.06-millisecond pulsar has three distinct components in its profile. As seen in Figure 3.1, the sharp trailing component (1) dominates at 575 MHz, but has a steeper spectrum than the other two, whose amplitude ratio remains approximately constant at all three frequencies. The two broader components precede the sharp component by $\sim 35°$and $80°$. Profiles presented in Bell *et al.* (1997) indicate that the trailing component continues to weaken at higher frequencies. For a classical triple profile with core and cone components, we would expect both conal outriders to strengthen relative to the central core at high frequencies. The widths of all three components are similar at the two lower frequencies, and sharper at 1410 MHz. The leading component is also closer to the others by $10°$ at this frequency. In the 820-MHz and 575-MHz profiles there is evidence for a small amount of emission following the strong sharp component. This also appears in shorter averages.

The 1410-MHz profile in Figure 3.2 shows no detectable polarization, although Xilouris *et al.* (1998) detected $\sim 25\%$ linear polarization. At both 820 and 575 MHz the strong trailing component is partially linearly polarized with $P \sim 25\%$. This same component displays a small amount of right-handed circular polarization at these frequencies, with $V \sim -10\%$. The PPA curve is only defined under this component, and appears similar for the two frequencies.

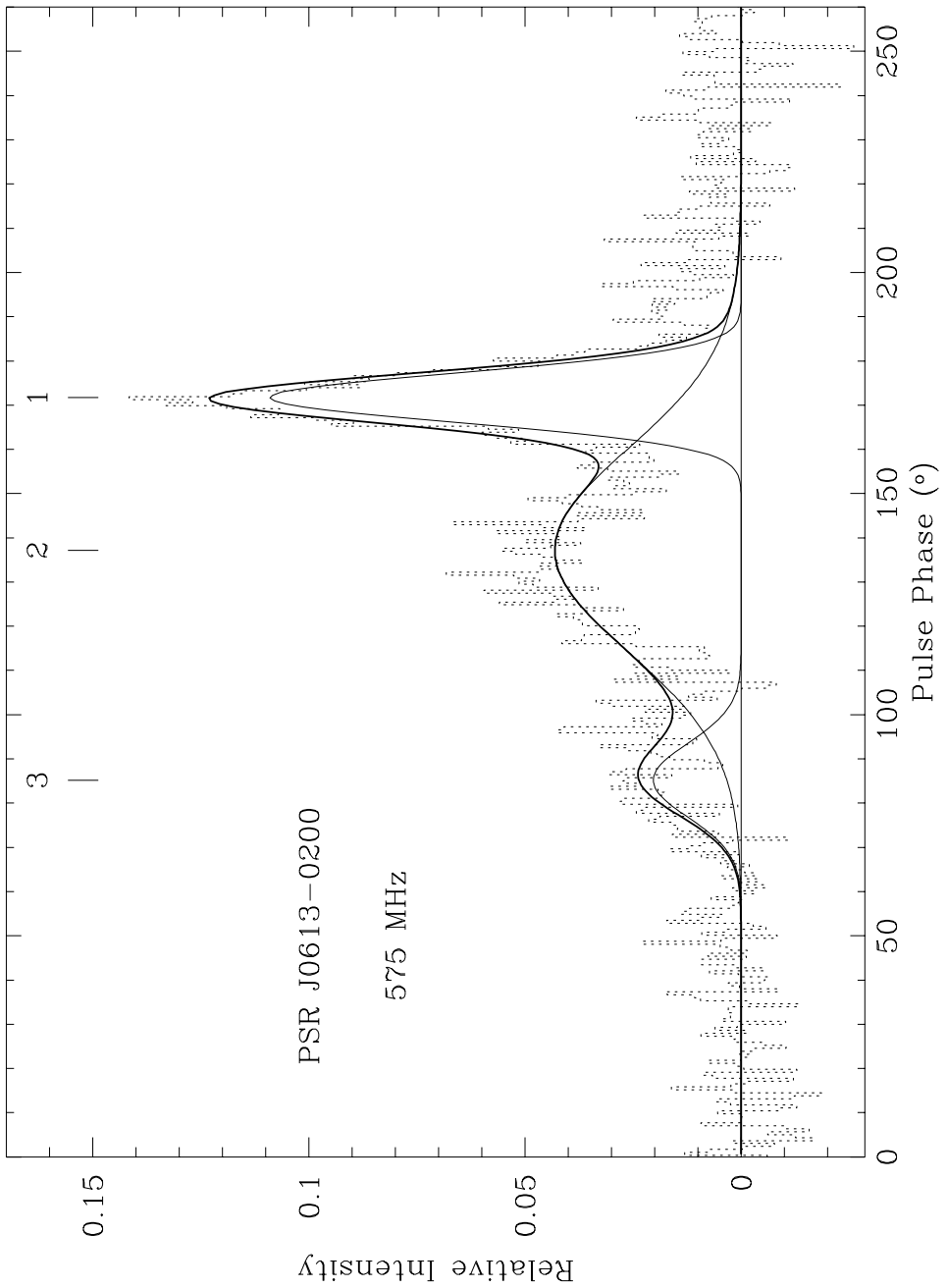


Fig. 3.1.— The Gaussian component decomposition for PSR J0613−0200 at 575 MHz is shown. The dotted histogram represents the data. The light solid lines are individual Gaussian components, whose sum is given by the dark solid line. Each component is identified with a number associated with the component number in Table 3.1.

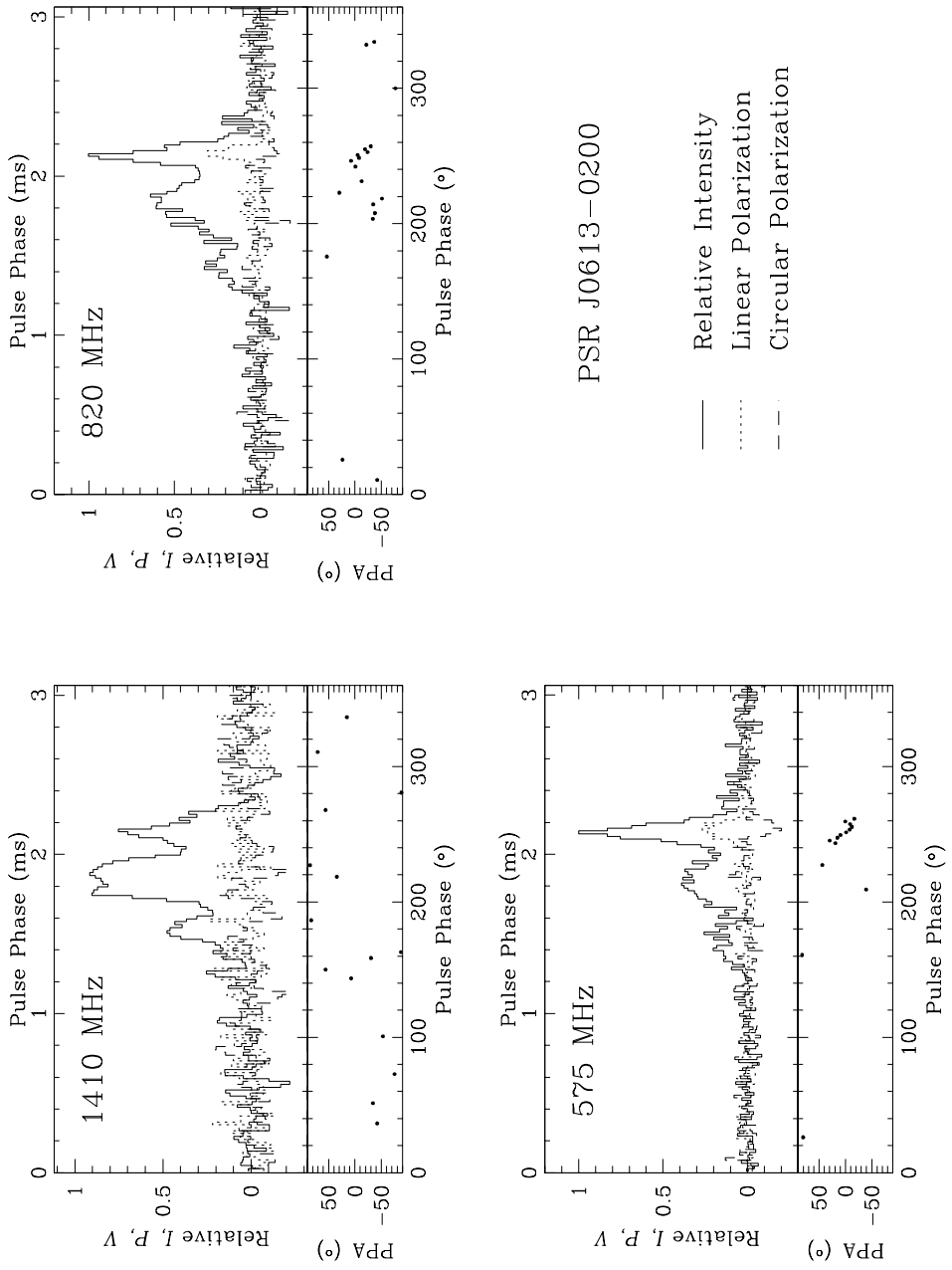


Fig. 3.2.— Polarization profiles of PSR J0613−0200 are displayed for three radio frequencies. For each one, the relative intensity, linear, and circular polarizations are plotted against pulse phase using solid, dotted, and dashed lines, respectively. The bottom axis indicates the pulse phase in degrees, while the top axis displays the same quantity in milliseconds. The polarization position angle (PPA) is plotted for phases where the linear polarization exceeds a certain threshold times the off-pulse *rms*. The resolution of the plots is given in Table 3.2, along with the integration time of the data presented, and the PPA threshold used. In this particular case, the 1410-MHz profile has been smoothed by an additional 3 time bins.

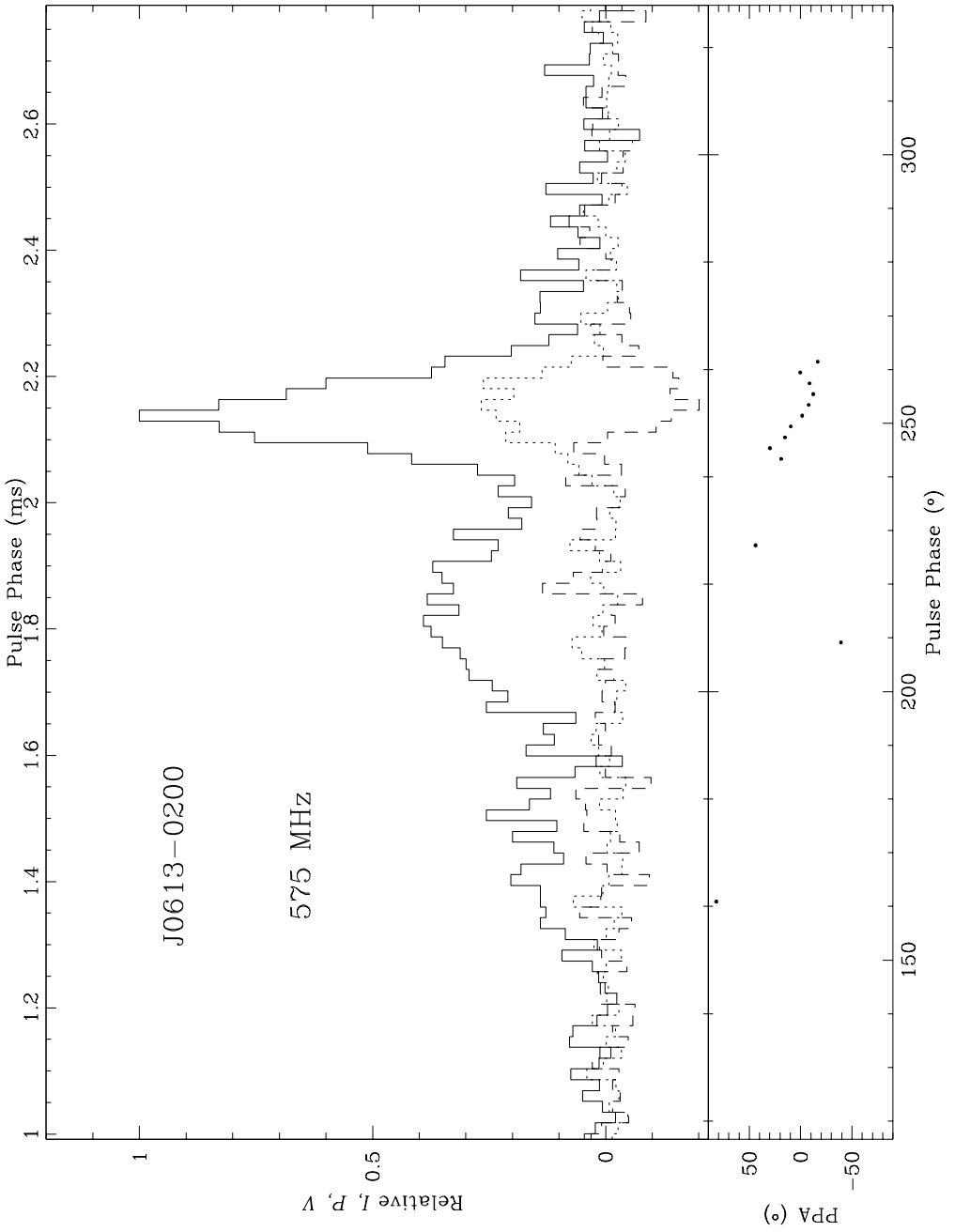


Fig. 3.3.— A region around the pulsed emission has been expanded in the 575-MHz polarization profile of PSR J0613−0200.

## 3.3 PSR J1012+5307

The profile of this pulsar is fairly complex, with many components in 3 distinct structures. The main pulse at 1410 MHz has at least 3 components, and is followed by a double-peaked interpulse (IPa), and then another weak component (IPb). Up to 7 Gaussians were required to achieve a reasonable fit to the intensity profile (cf. Figure 3.4), while Kramer *et al.* (1998) fits the profile at 1410 MHz with 9 Gaussian components (the two extra components accounted for low-level emission which is not obvious in our data, which have lower $SNR$). Emission is present over a wide range of longitudes, which may indicate that the emission is all from a single pole. The $\sim 180^\circ$ separation between the MP complex and IPb supports a classic two-pole pulse/interpulse morphology, however. The trailing component of the main pulse, and the double-peaked IPa strengthen relative to the other components with increasing radio frequency. IPb strengthens relative to the other components with decreasing radio frequency. The separations between the various components are not a strong function of observing frequency.

The last component of the main pulse (1) is highly linearly polarized. Significant linear polarization is also seen in the two interpulse structures. The leading edge of the MP is weakly polarized, becoming less polarized with increasing radio frequency. Sense-reversing circular polarization is associated with the main pulse at all frequencies. Both interpulse structures also show evidence for weak sense-reversing circular polarization (cf. Figure 3.6). The PPA curve is very flat.

A separate profile at 1410 MHz taken in 1996 October with the EBPP displays a similar intensity profile, circular polarization, and PPA curve, but the trailing component of the main pulse structure is even more linearly polarized ($\sim 70\%$) than that displayed here ($\sim 60\%$, cf. Figure 3.5). The linear polarization of IPb is also stronger in this profile. The data at the lower frequencies are too weak to place useful limits on polarization variations between observations.

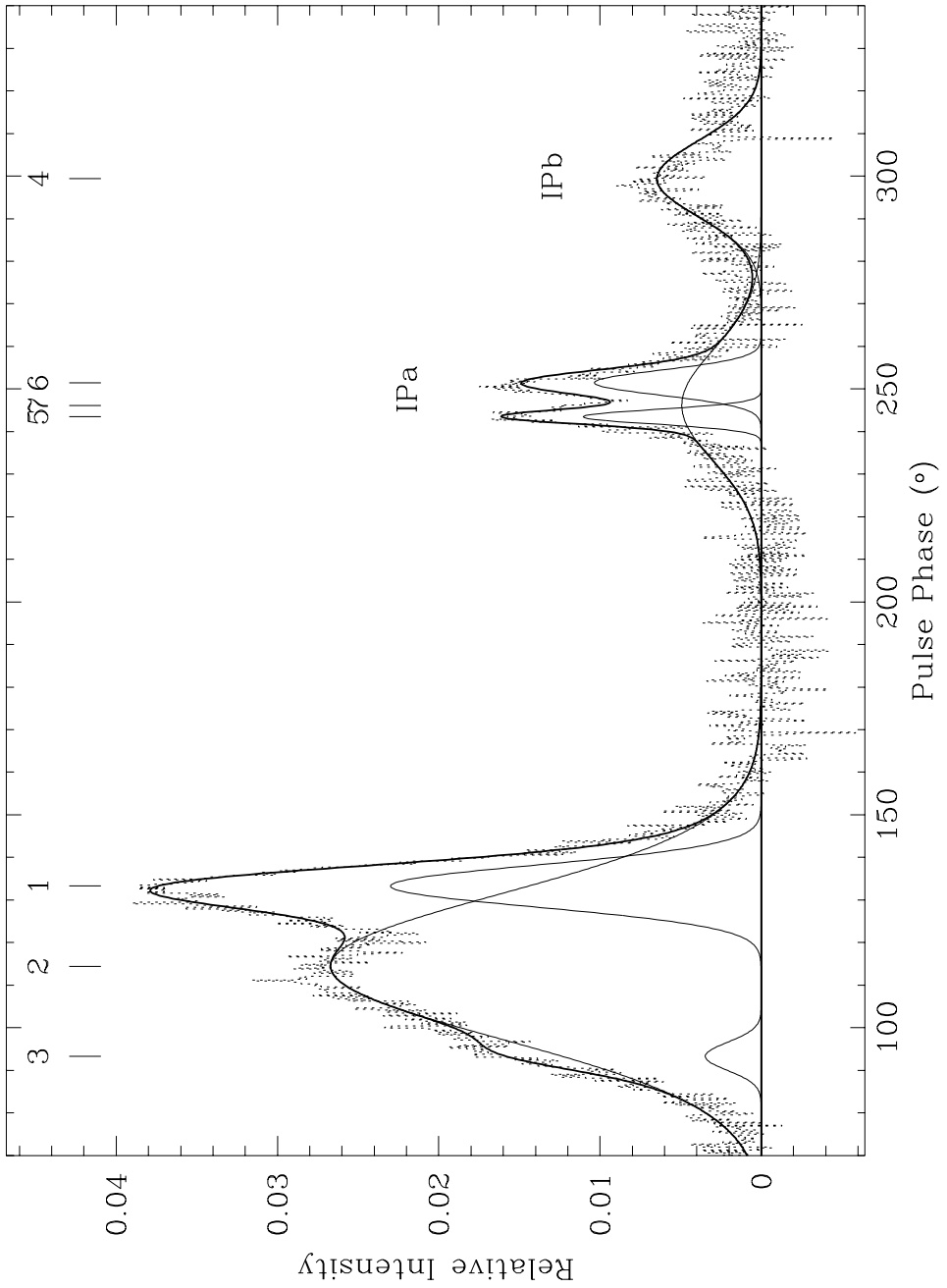


Fig. 3.4.— The Gaussian component decomposition for PSR J1012+5307 at 1410 MHz is shown. See the caption of Figure 3.1 for details.

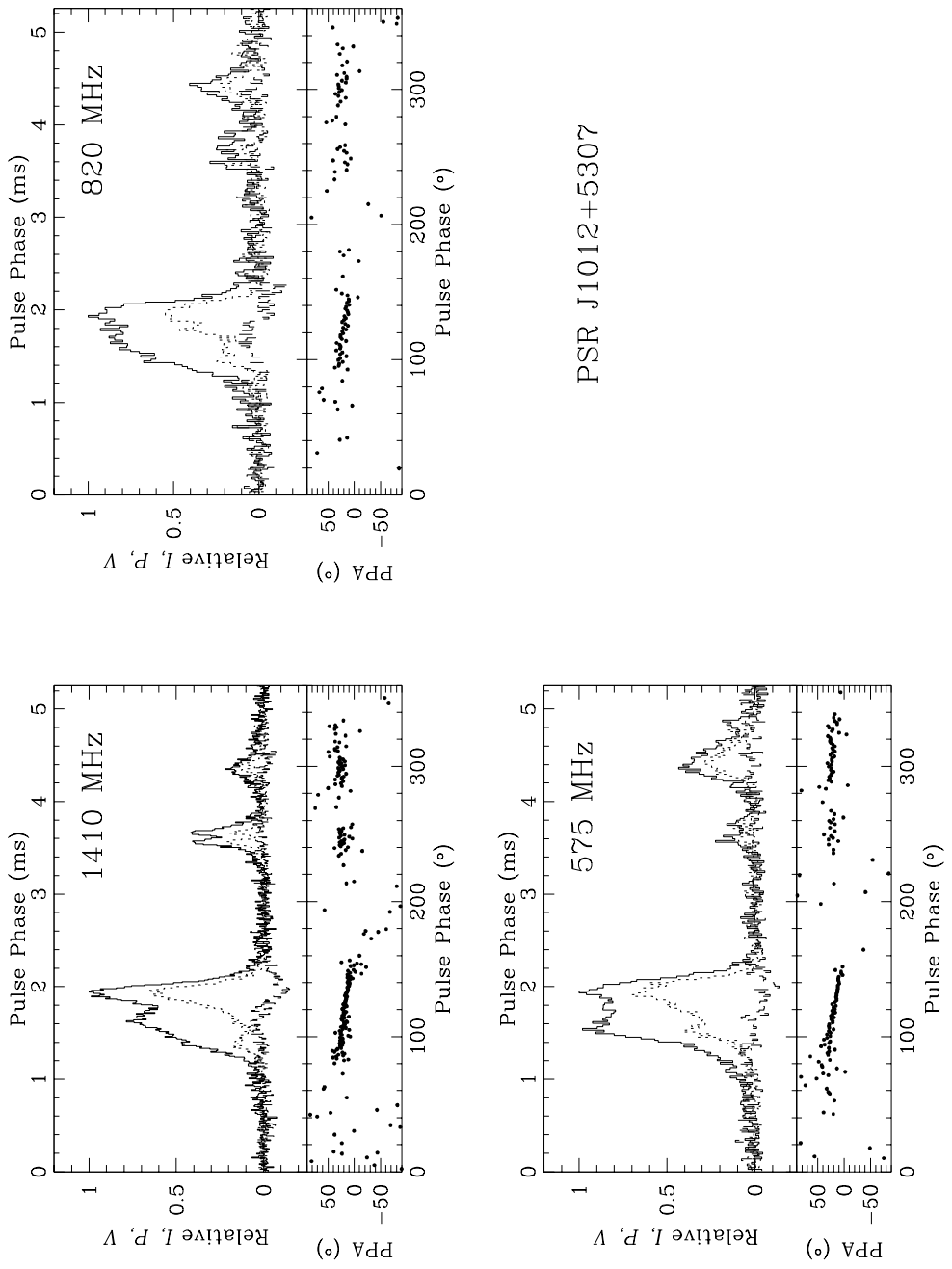


Fig. 3.5.— Polarization profiles of PSR J1012+5307 are displayed for three radio frequencies. See the caption of Figure 3.2 for details.

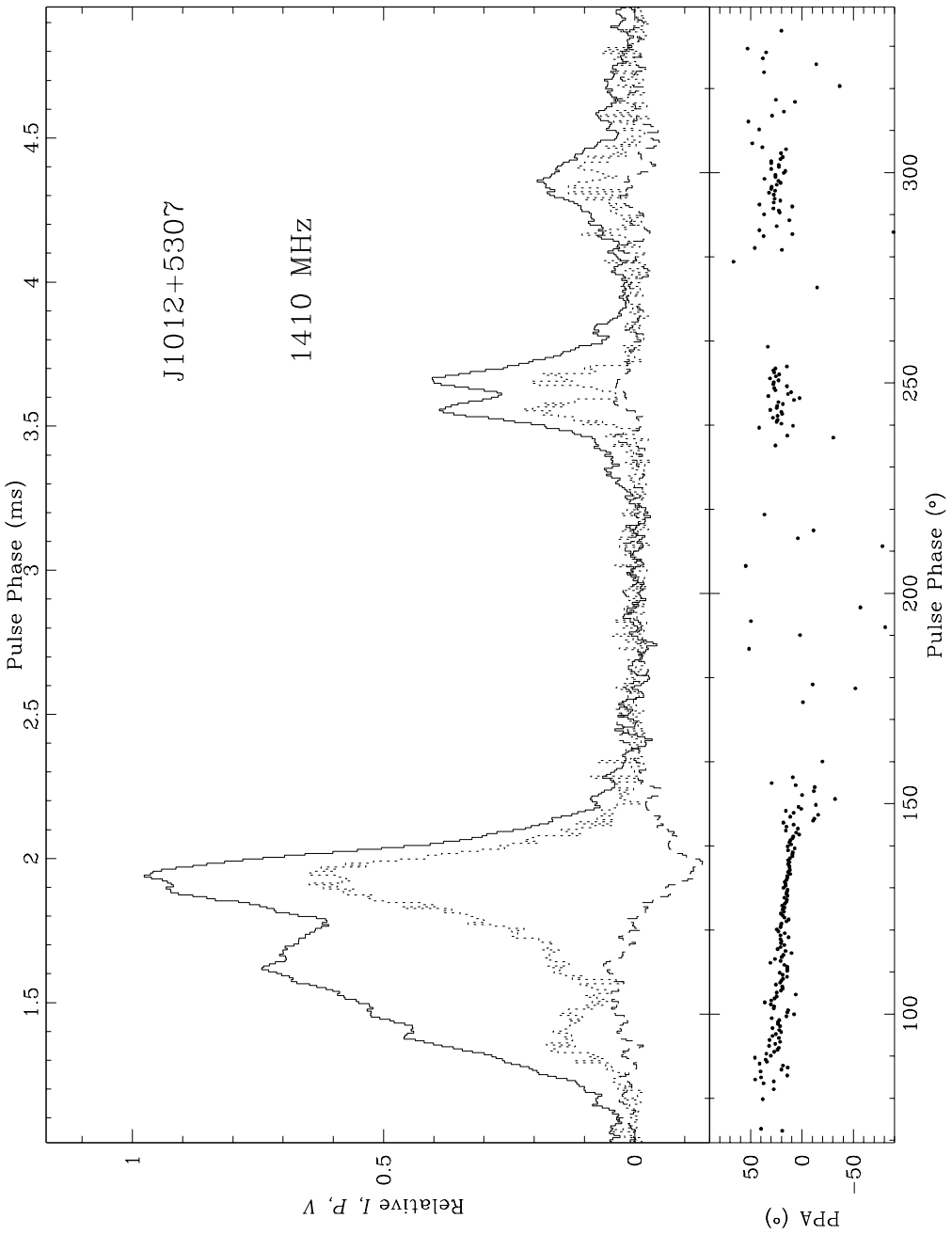


Fig. 3.6.— A region around the pulsed emission has been expanded in the 1410-MHz polarization profile of PSR J1012+5307. The resolution of this profile is 6.9$\mu$s. The data have also been smoothed by 5 time bins.

## 3.4 PSR J1022+1001

The intensity profile of this pulsar can be fit at all three frequencies by a sharp trailing component (1), a relatively sharp component (2) which precedes this by $\sim 11°$, a small sharp component (4) between the two, and a broad leading component (3) which precedes the others by $\sim 20°$. In general, the trailing component is more dominant at low frequencies (cf. Figure 3.8), but the intensity ratio of the two main components is not constant in time. This ratio varies on a time scale of hours at 430 MHz (Camilo 1995), and also changes at 1410 MHz (Kramer *et al.* 1998). At 1.7 GHz, however, the leading component is usually brighter, (Camilo *et al.* in prep), and at 4.85 GHz (Kijak *et al.* 1997), the trailing component has faded with respect to the leading one. The averages for this object look much the same from epoch to epoch, with the 1410-MHz data from 1996 October being indistinguishable from the results displayed here. Inspection of daily averages of our data reveal, however, that at 1410 MHz, the component ratio of the two main peaks varies slightly from day to day, while at 820 MHz, it reverses for a single day, with the trailing component stronger the remainder of the time. The trailing component is also stronger for each daily average of 575-MHz data. The overall average profile development is not consistent with normal triple or multiple profile frequency development.

The sharp trailing component (1) is highly linearly polarized at all RFs (75%). The early portion of the profile is also linearly polarized, although more weakly. The pulsar seems to be most weakly polarized at 820 MHz, but as noted by Xilouris *et al.* (1998) and Sallmen *et al.* (1997) the polarization of this pulsar is not constant, changing with the profile variations. The PPA curve is well defined, but with an orthogonal mode transition associated with the leading main component, and accompanied by depolarization. The circular polarization is small or non-existent for the leading portion of the pulse, but is about $-20\%$ on the trailing edge of the leading main component, and $-15\%$ under the trailing sharp component.

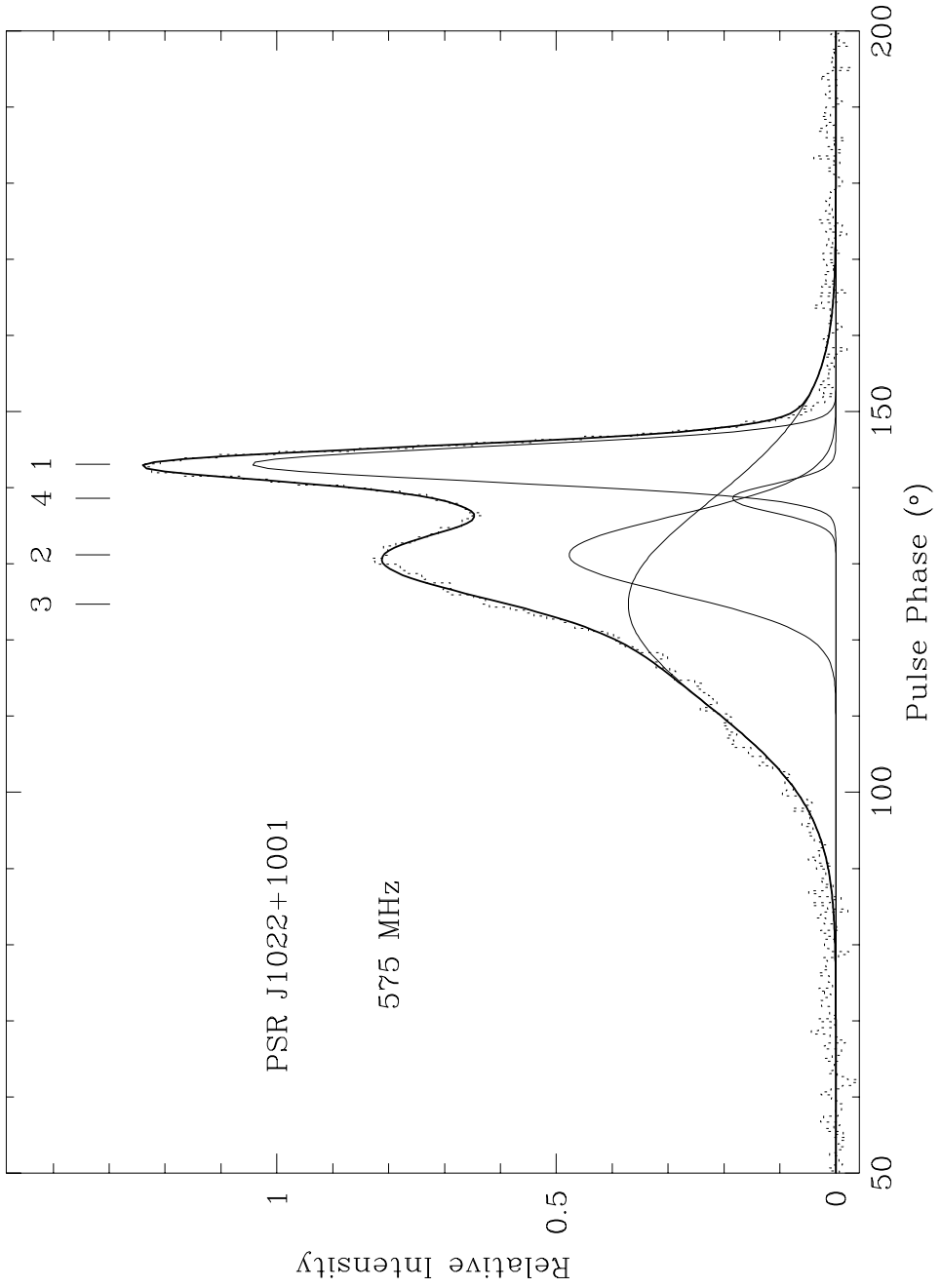


Fig. 3.7.— The Gaussian component decomposition for PSR J1022+1001 at 575 MHz is shown. See the caption of Figure 3.1 for details.

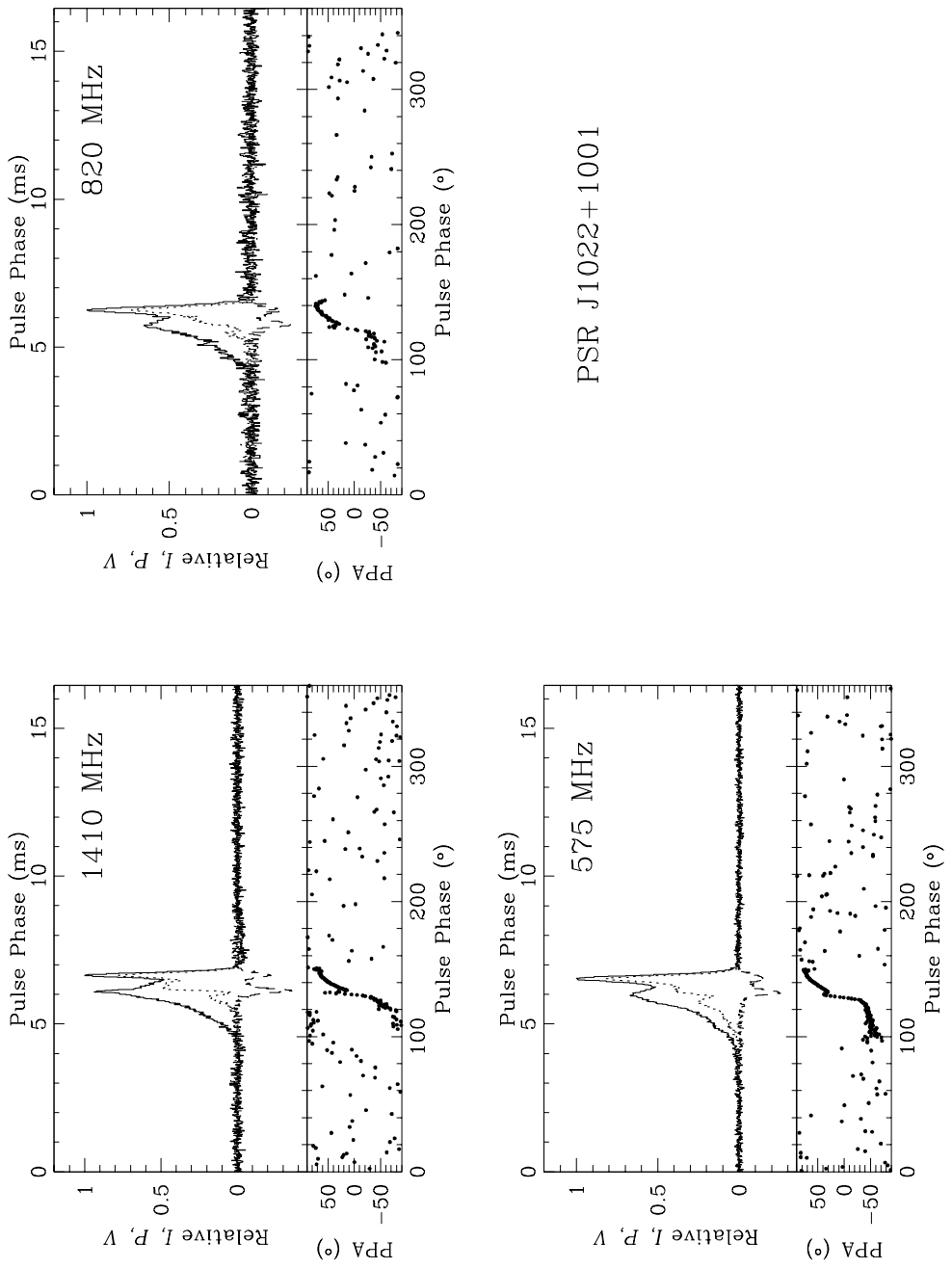


Fig. 3.8.— Polarization profiles of PSR J1022+1001 for three radio frequencies. See the caption of Figure 3.2 for details.

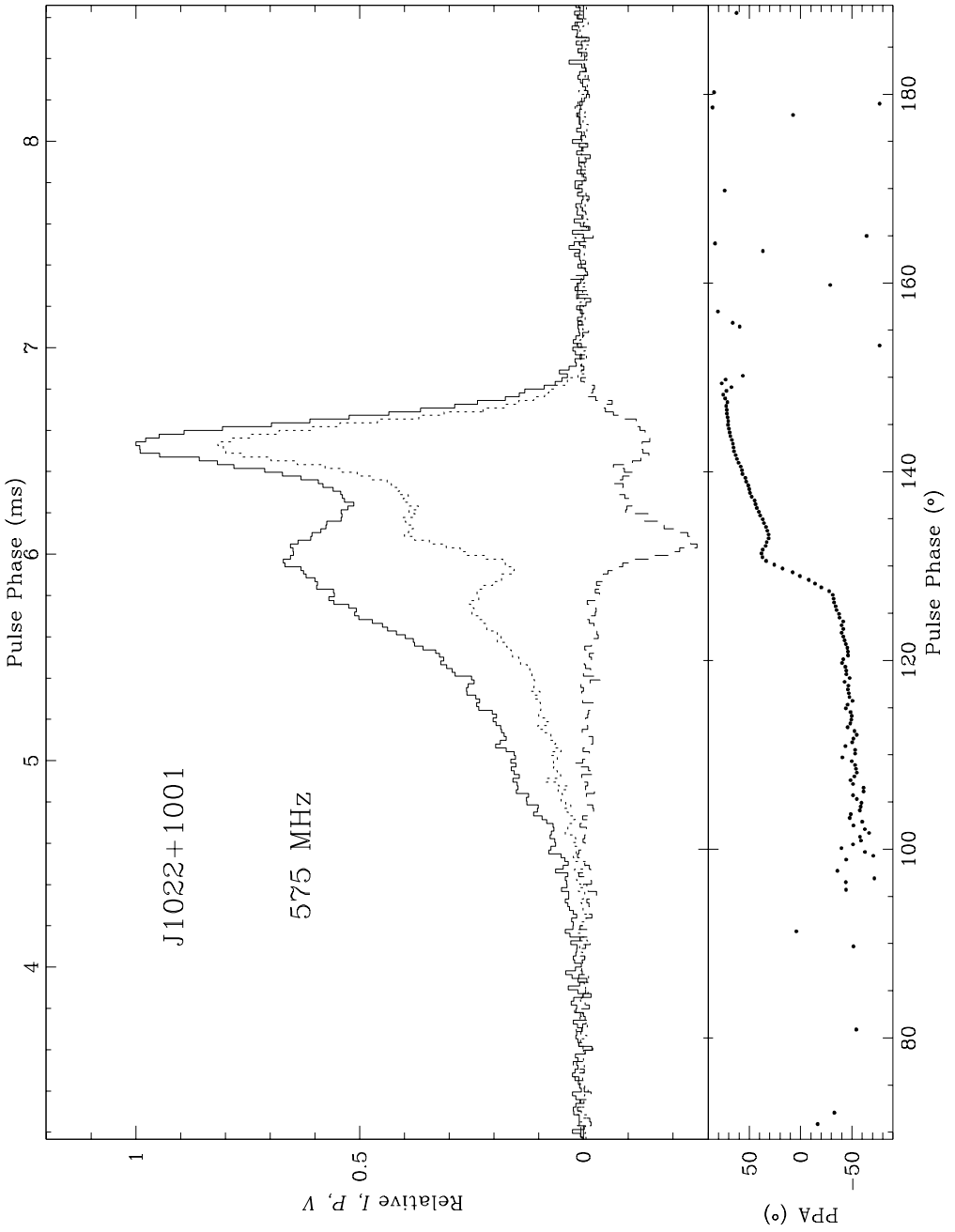


Fig. 3.9.— A region around the pulsed emission has been expanded in the 575-MHz polarization profile of PSR J1022+1001.

## 3.5 PSR B1620−26

The profile of this 11.1-millisecond pulsar shows 3 components, apparently a core component (1) with conal outriders. The strongest central component shows significant linear polarization, increasing with increasing radio frequency to about 40% at 1410 MHz (cf. Figure 3.11. This is larger than that seen by Xilouris *et al.* (1998), indicating possible variations in the polarization of this pulsar. The signal to noise of short term averages of our data is insufficient to place interesting limits on possible polarization variations.

The trailing component shows no polarization, while the leading component is somewhat linearly polarized. The circular polarization of the central component is $\sim -20\%$, but is negligible for the surrounding components. The PPA curve is well defined, with an orthogonal mode change occurring between the first and second components, accompanied by a decrease in linear polarization. All of these properties are consistent with a classical triple profile. The central component becomes *stronger* at high frequencies, in contrast to the expected behaviour. In addition, there is no significant frequency development of component separations or widths. The two outriders are always $\sim 20^\circ$ on either side of the central component, and the trailing component is always slightly weaker than the preceding one.

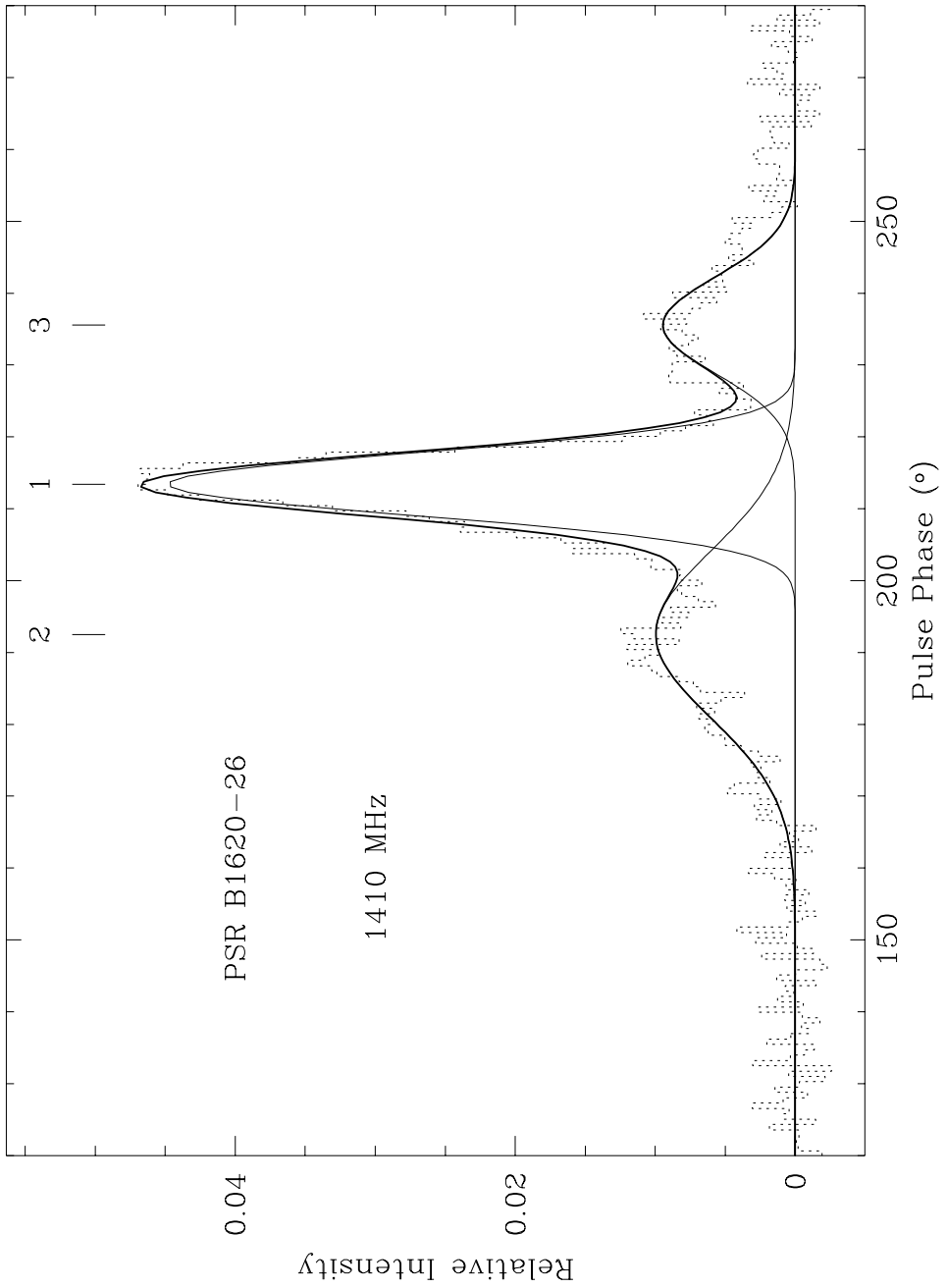


Fig. 3.10.— The Gaussian component decomposition for PSR B1620−26 at 1410 MHz is shown. See the caption of Figure 3.1 for details.

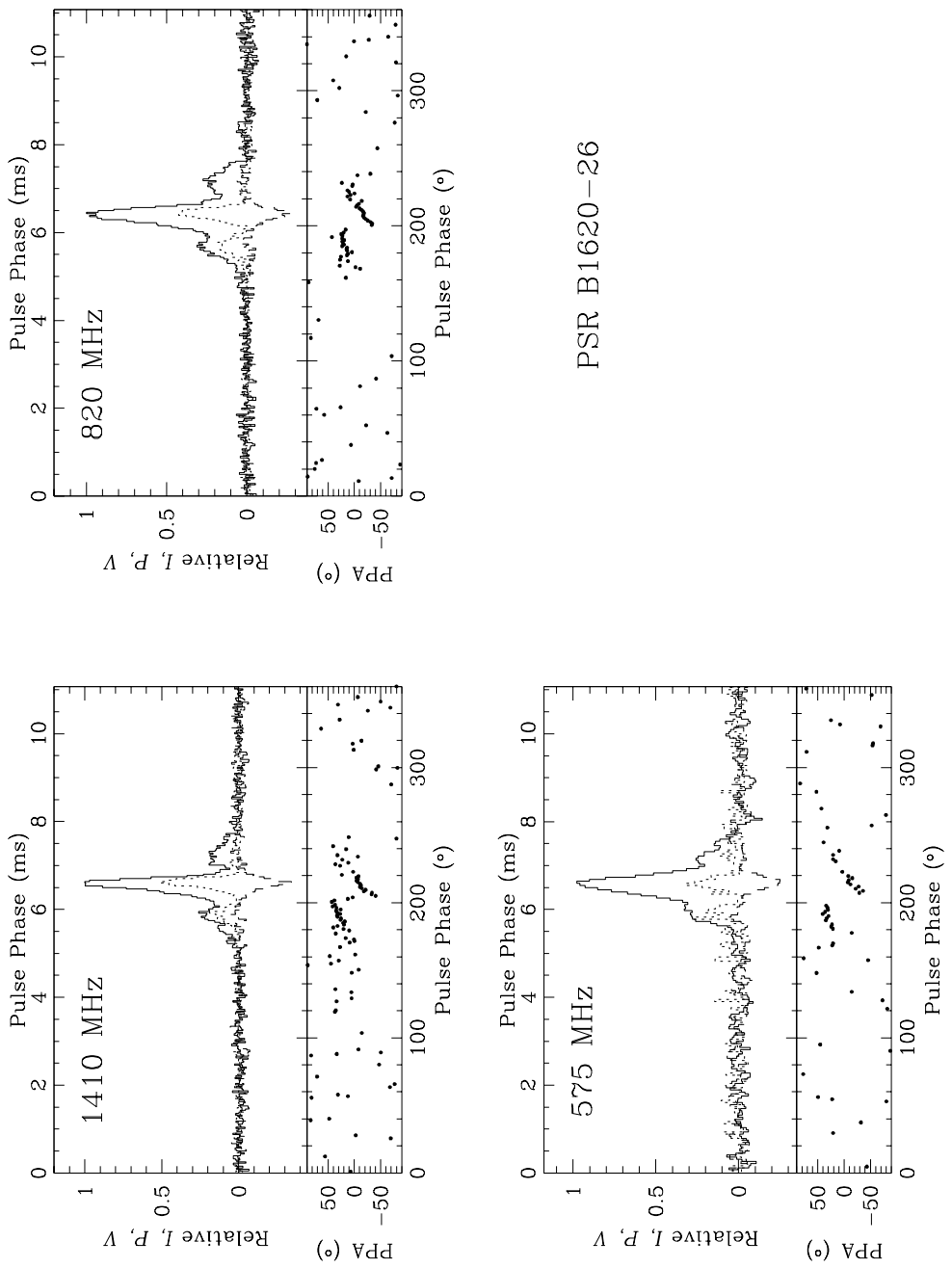


Fig. 3.11.— Polarization profiles of PSR B1620−26 for three radio frequencies. See the caption of Figure 3.2 for details. In this particular case, the 575-MHz profile has been smoothed by an additional 3 time bins.

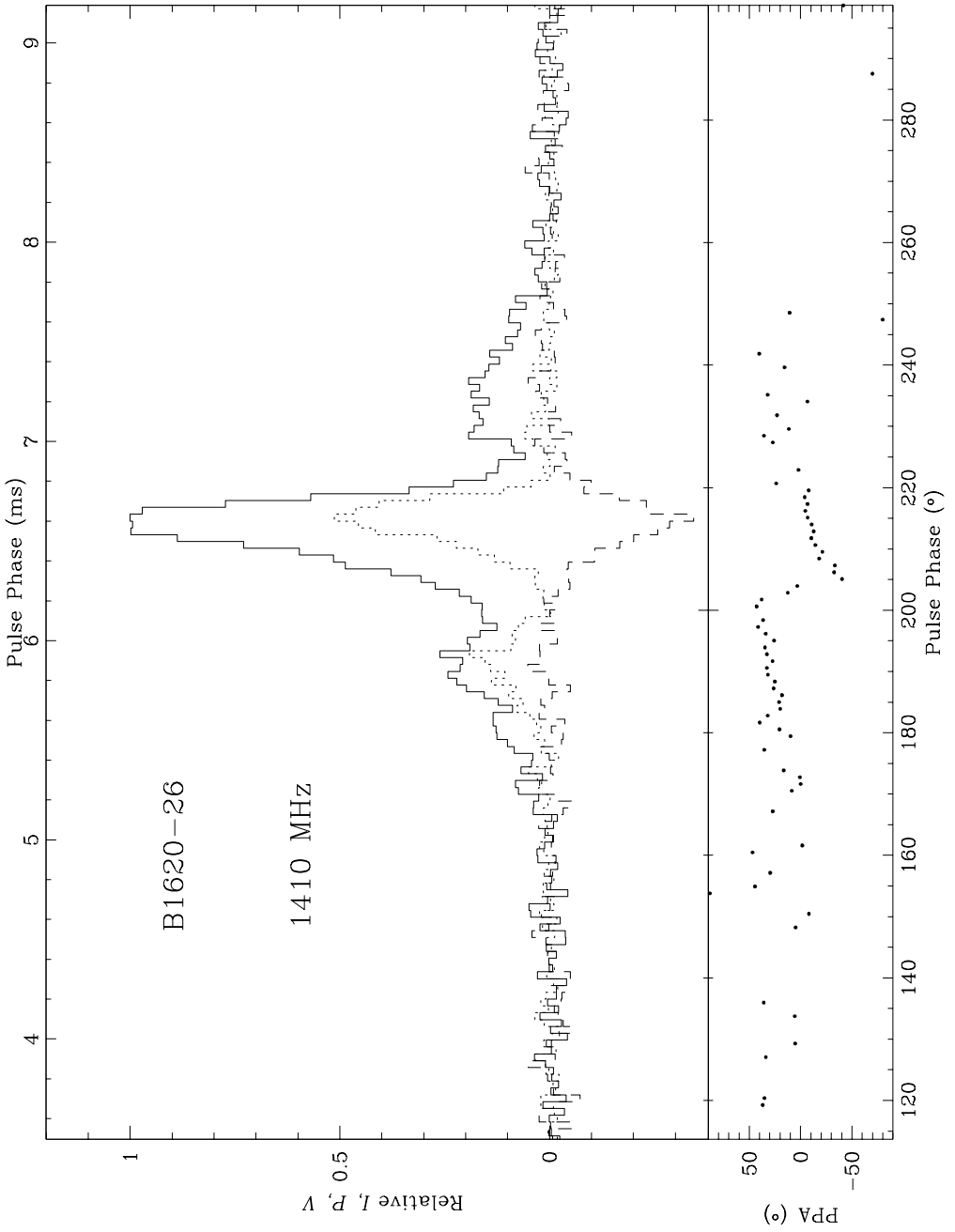


Fig. 3.12.— A region around the pulsed emission has been expanded in the 1410-MHz polarization profile of PSR B1620−26.

## 3.6 PSR J1713+0747

At 1410 MHz, the profile of this 4.5-millisecond pulsar has many components within a single structure, as can be seen in Figure 3.13. Six Gaussian components were required to fit the 1410-MHz data of Kramer *et al.* (1998). The same is true here. The shape of the overall profile is fairly similar at all frequencies, although the small preceding and trailing components are more important at 2.38 and 4.85 GHz (Camilo 1995, Kijak *et al.* 1997). The apparent broadening of the profile at the lower frequency is not due to interstellar broadening, but the increased importance of the trailing components.

The leading components are significantly linearly polarized at 1410 MHz, while the trailing component shows only weak polarization. At 575 MHz and 820 MHz, the small preceding component is weakly polarized. Modest linear polarization occurs under the main peak at all frequencies, as seen in Figure 3.14. The peak linear polarization is $\sim 20 - 40\%$, with the lowest values occurring at 820 MHz. This does not agree with the expected depolarization with increasing radio frequency. The low linear polarization at 820 MHz is present in data from each of the three separate 1997 observing runs. However, Figure 3.16 displays a profile from February 1995, taken in the circular polarization basis. Significant linear polarization is present under the main peak. Only two of our observations of this pulsar near 800 MHz display a significantly larger degree of linear polarization than that of the average in Figure 3.14. No similar variations were observed at the other frequencies.

Weak sense-reversing circular polarization is centered near the main peak, identifying it as a core component. The PPA curve is relatively flat, but is disturbed by orthogonal mode changes which occur on either side of the main pulse, and are associated with drops in the linear polarization. The second orthogonal mode change is also associated with the sense-reversal of the circular polarization.

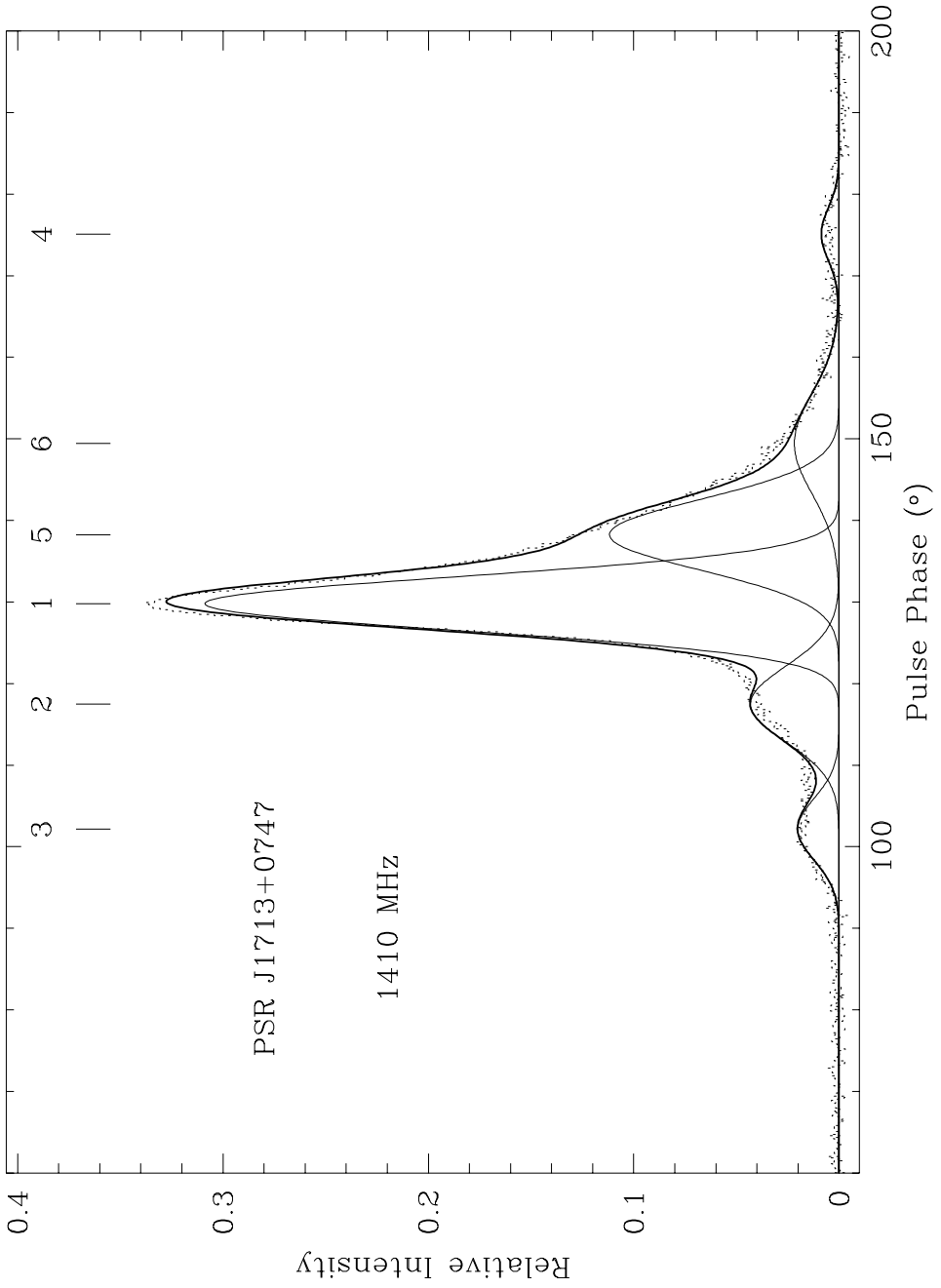


Fig. 3.13.— The Gaussian component decomposition for PSR J1713+0747 at 1410 MHz is shown. See the caption of Figure 3.1 for details.

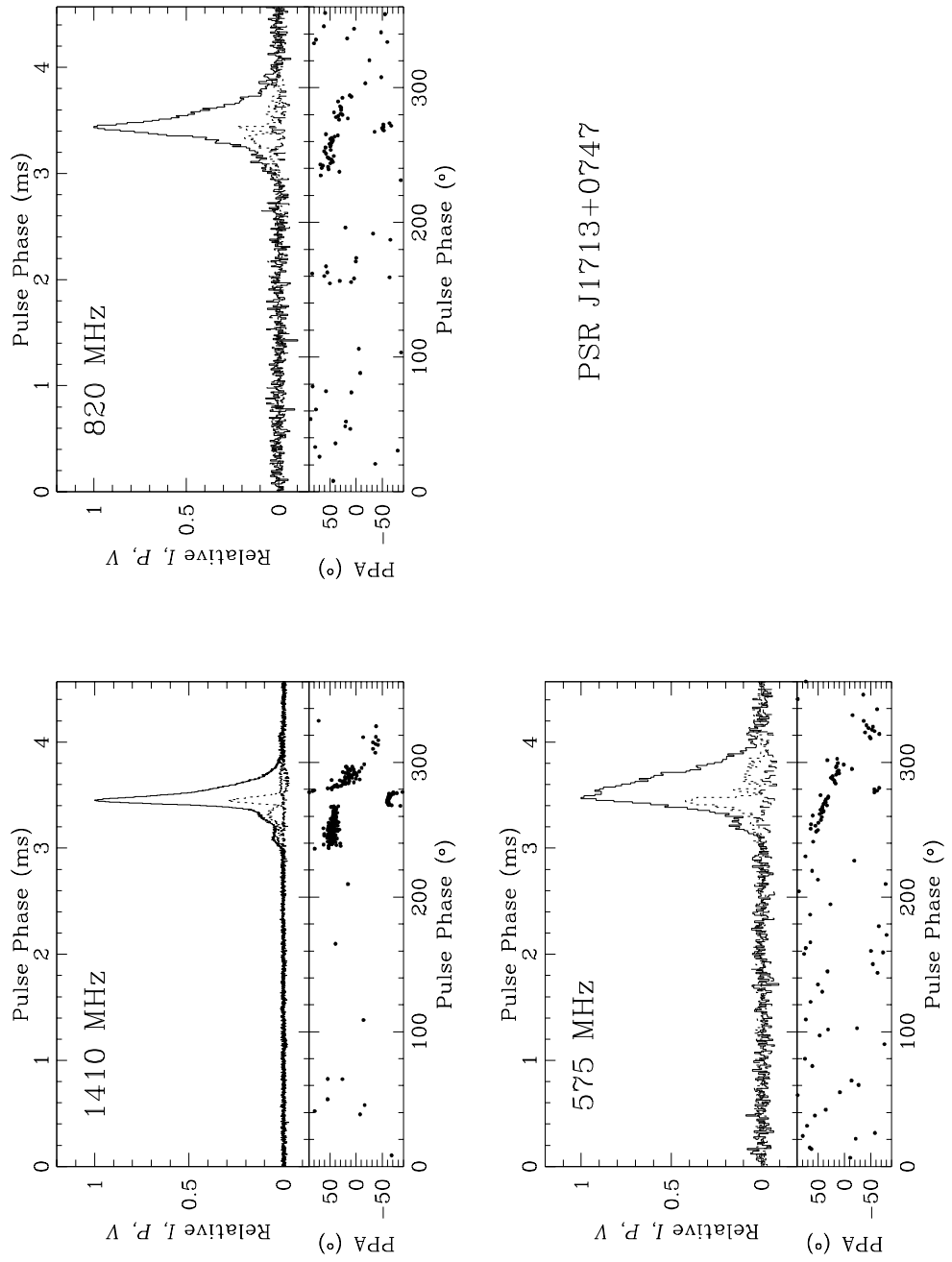


Fig. 3.14.— Polarization profiles of PSR J1713+0747 for three radio frequencies. The apparent sweep in the 1410-MHz PPA at 280° is due to a slightly incorrect instrumental correction for $\sigma$, combined with the extremely low linearly polarized fraction at that longitude. The PPA undergoes a second orthogonal mode transition at this longitude. See the caption of Figure 3.2 for details.

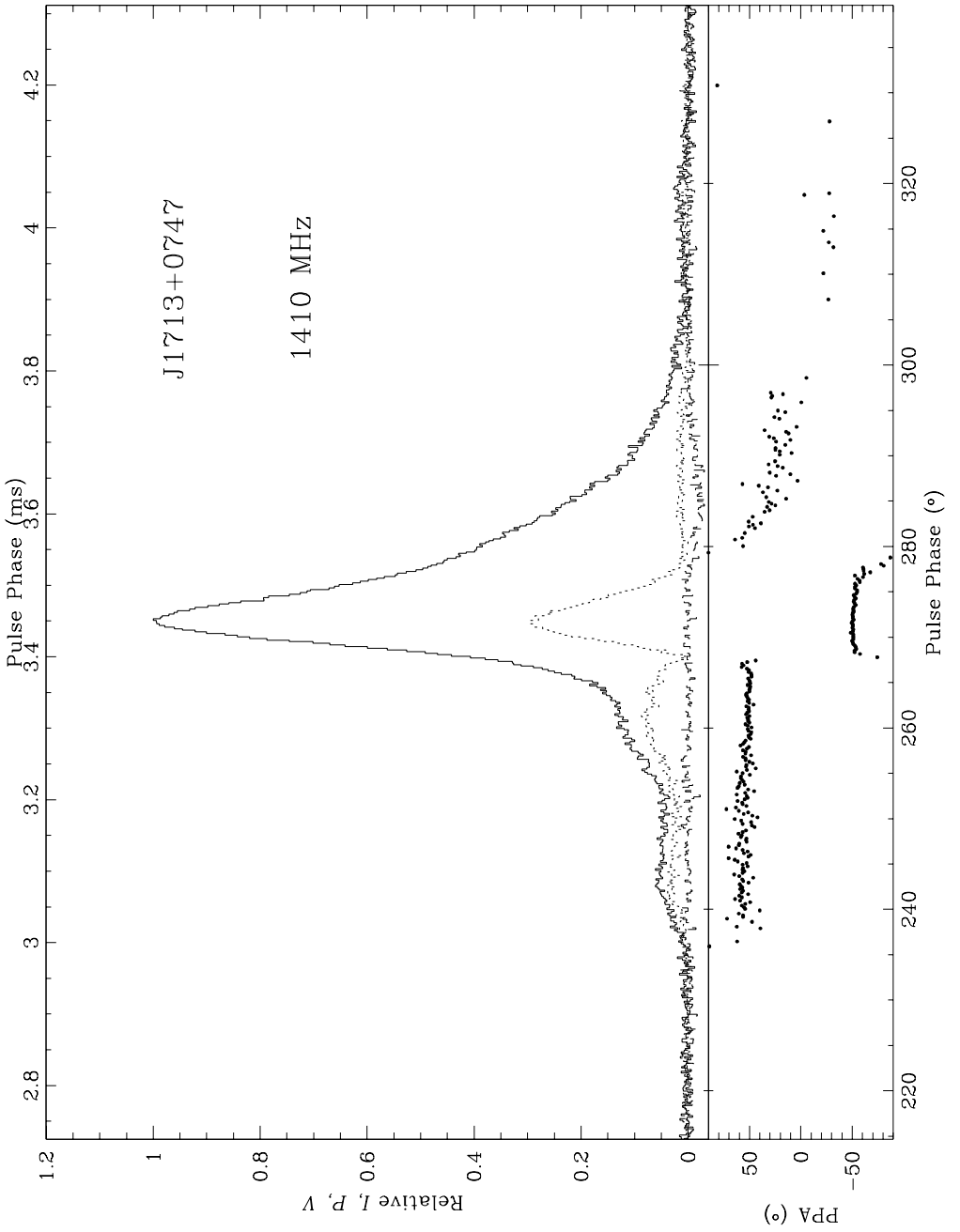


Fig. 3.15.— A region around the pulsed emission has been expanded in the 1410-MHz polarization profile of PSR J1713+0747.

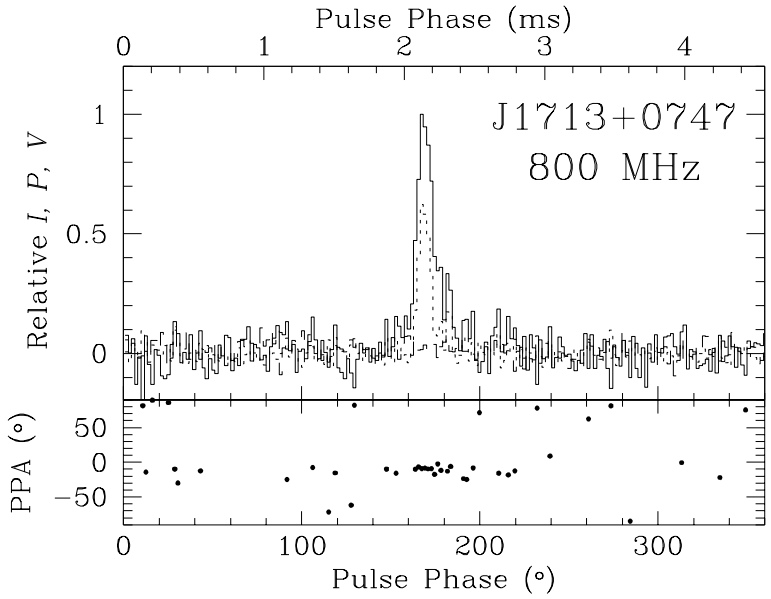


Fig. 3.16.— Polarization profile of PSR J1713+0747 at 800 MHz. This observation has a higher linearly polarized fraction than that typically seen at 820 MHz. See the caption of Figure 3.2 for details.

## 3.7 PSR J1730−2304

The profile presented in Figure 3.17 shows a clear triple structure at 1410 MHz, plus small outer components. Kramer *et al.* (1994) fit five Gaussians to the intensity profile; here only four were required, as the trailing component is quite weak. The central component (2) is less prominent at higher frequencies, behaviour which is consistent with a core/cone interpretation of this profile. As is expected for a symmetric triple or multiple profile, the separation of the three main components decreases with increasing radio frequency, The width of the central component decreases slightly with frequency, as does that of the small preceding component (4). No significant width change is seen in the other two main components (2,3). The central feature seems delayed relative to the symmetry center of the profile at lower frequencies.

The pulsar is only modestly linearly polarized in all the data displayed here, and increases with increasing radio frequency, contrary to expectation. Little or no polarization is associated with the central component. The relatively small polarized fraction is in sharp contrast to the 1410-MHz profile presented by Xilouris *et al.* (1998), which is almost 100% polarized for the outer components of the triple. This is undoubtedly a reflection of the profile mode changes discussed therein, in which variations of the linear polarization from 0-100% are associated with profile shape variations. The circular polarization was found to remain relatively stable.

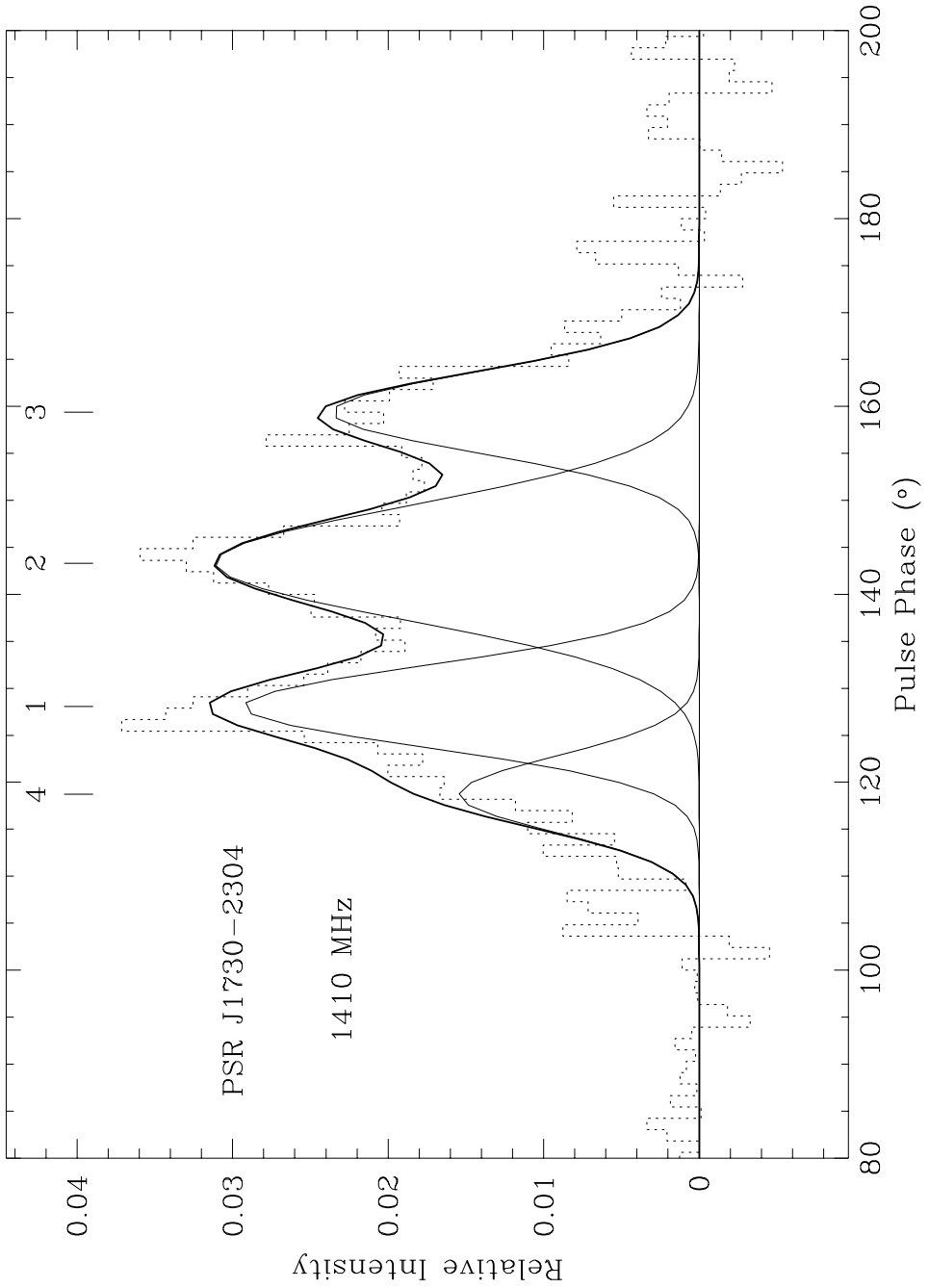


Fig. 3.17.— The Gaussian component decomposition for PSR J1730−2304 at 1410 MHz is shown. See the caption of Figure 3.1 for details.

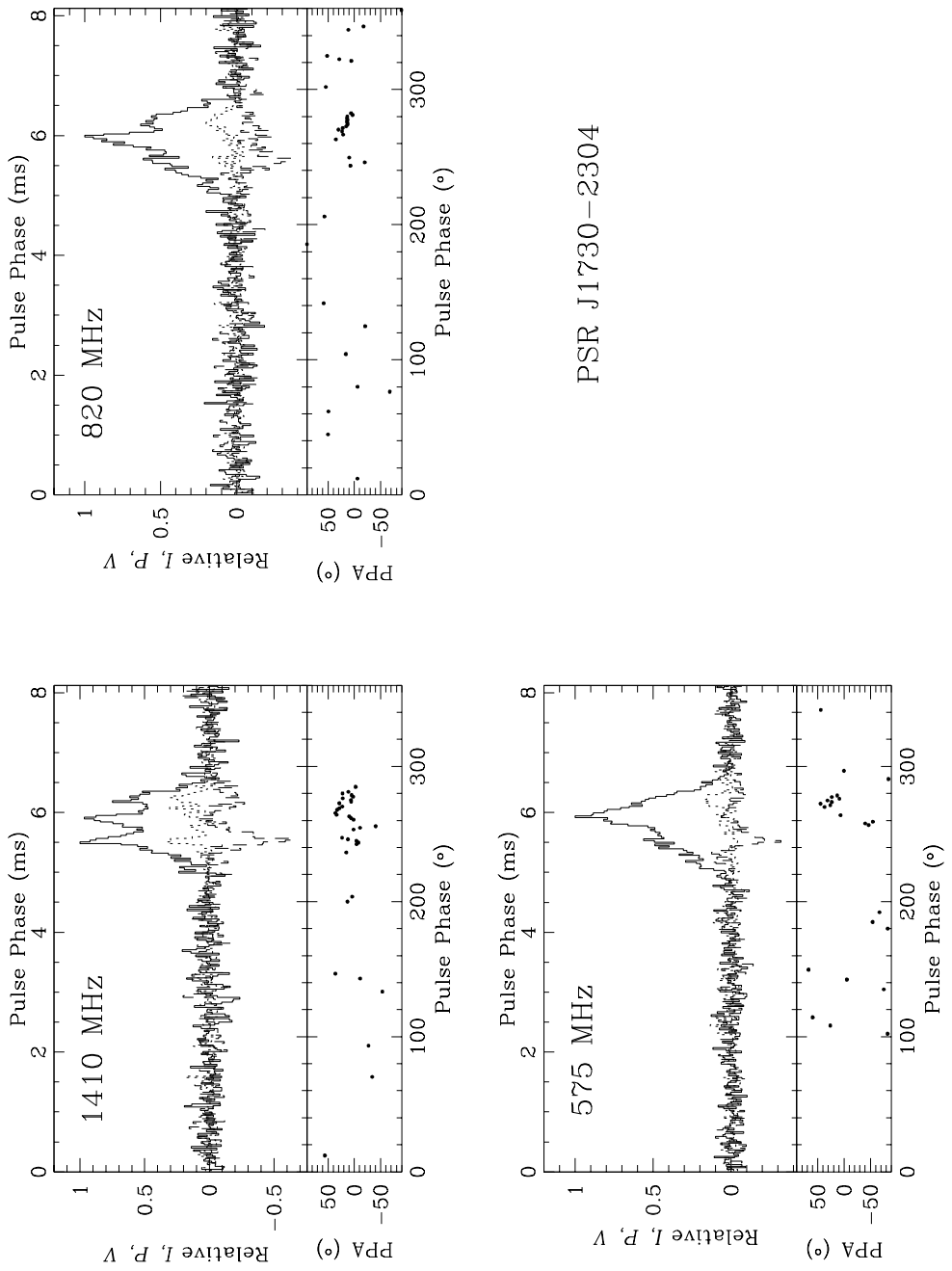


Fig. 3.18.— Polarization profiles of PSR J1730−2304 for three radio frequencies. See the caption of Figure 3.2 for details.

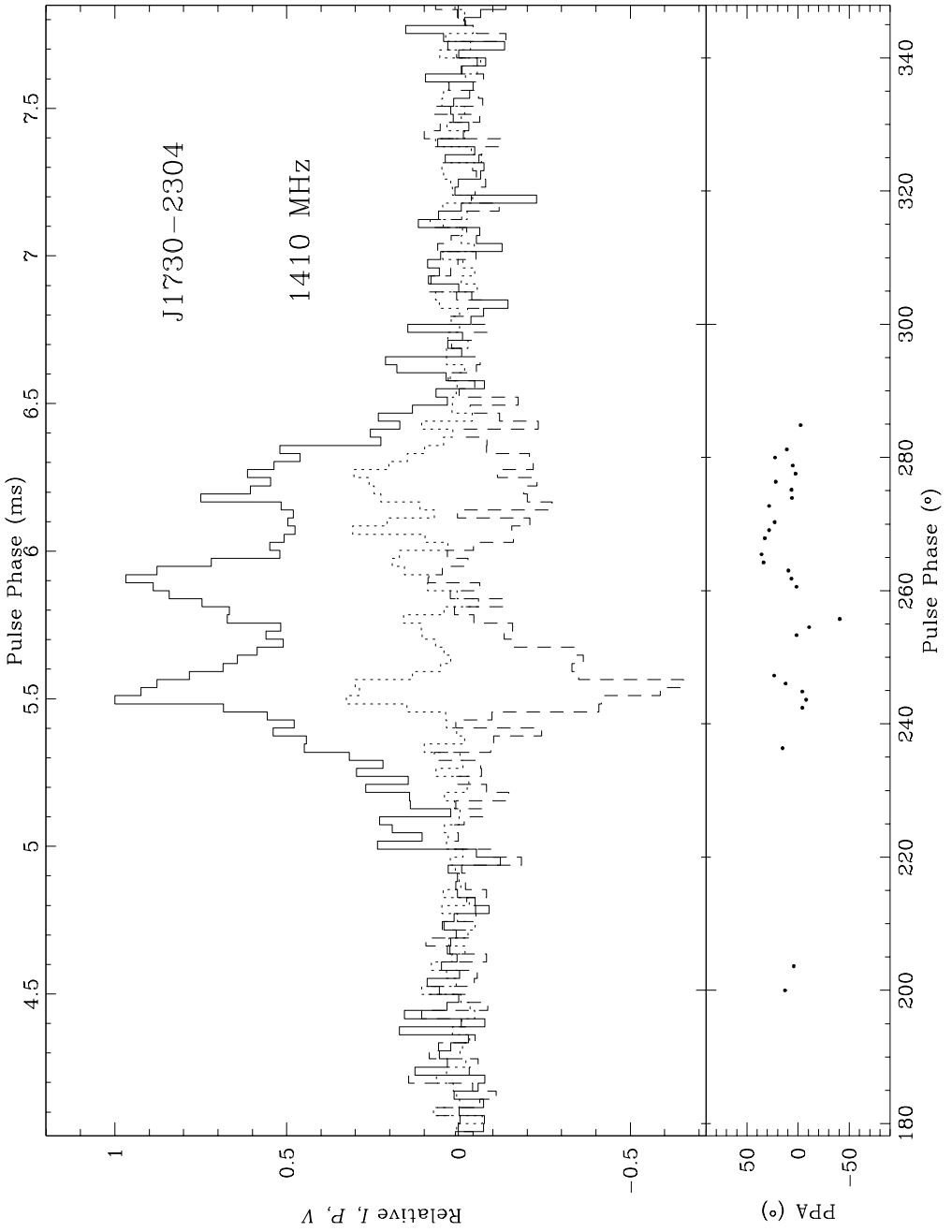


Fig. 3.19.— A region around the pulsed emission has been expanded in the 1410-MHz polarization profile of PSR J1730−2304.

Despite the expectation from this that the circular polarization displayed here should match the $\approx 10\%$ shown in the 1410-MHz profile of Xilouris *et al.* (1998), the leading component of this profile has a circular polarization of $-50\%$. Due to the low level of linear polarization in this profile, the PPA curve is poorly defined, although it is consistent with the published data. At 575 MHz, the only linear polarization is on the trailing edge of the profile, while moderate circular polarization is seen.

## 3.8 PSR B1821−24

This 3-millisecond pulsar has a three component profile (cf. Figure 3.20). Two sharp components (1,2) are separated by approximately 108 degrees, and are followed by a weaker broad component, about 180° from the first component. At 1410 MHz, an extra broad component under the second peak was required to explain the pulse shape. The component separations are frequency-independent, suggesting a possible two-pole model for the pulsar.

The profile is significantly broadened due to interstellar scattering at lower frequencies. This is reflected in the component widths listed in Table 3.1. The 1410-MHz widths for components 1 and 2 are consistent with the 1330-MHz component widths measured by Foster, Fairhead & Backer (1991). The component separations also agree. The second component becomes increasingly dominant at higher frequencies, so that by 1410 MHz it has become the largest component. Backer & Sallmen (1997) have reported that this pulsar undergoes mode changes at 1400 MHz. About one-third of the time, this component is much weaker relative to the other two, whose intensity ratio remains roughly constant. No such variations were seen in their data at 800 MHz. Figure 3.23 displays results that indicate that the component ratios do vary at this frequency. In 1997 July, an apparent increase in the relative strength of the broad component was seen which can be explained if the two sharp components are broadened due to increased interstellar scattering at this epoch. The second component is, however, stronger relative to the first at this epoch.

The two sharp components are both strongly linearly polarized (40-60%), while the third broad component is unpolarized. No significant circular polarization is present. Under each component, the PPA curve is relatively flat, with an offset of about 40 degrees between the two.

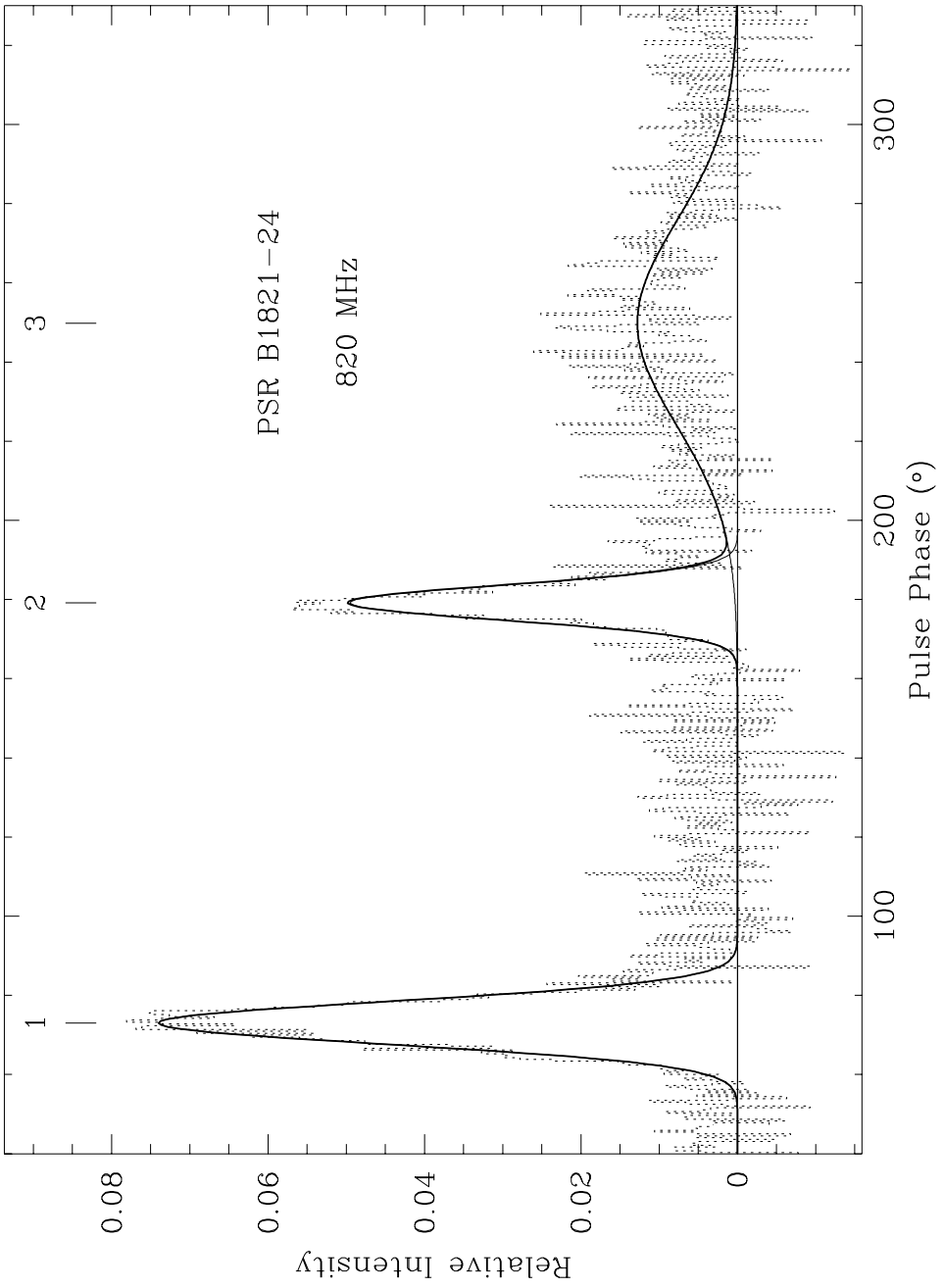


Fig. 3.20.— The Gaussian component decomposition for PSR B1821−24 at 820 MHz is shown. See the caption of Figure 3.1 for details.

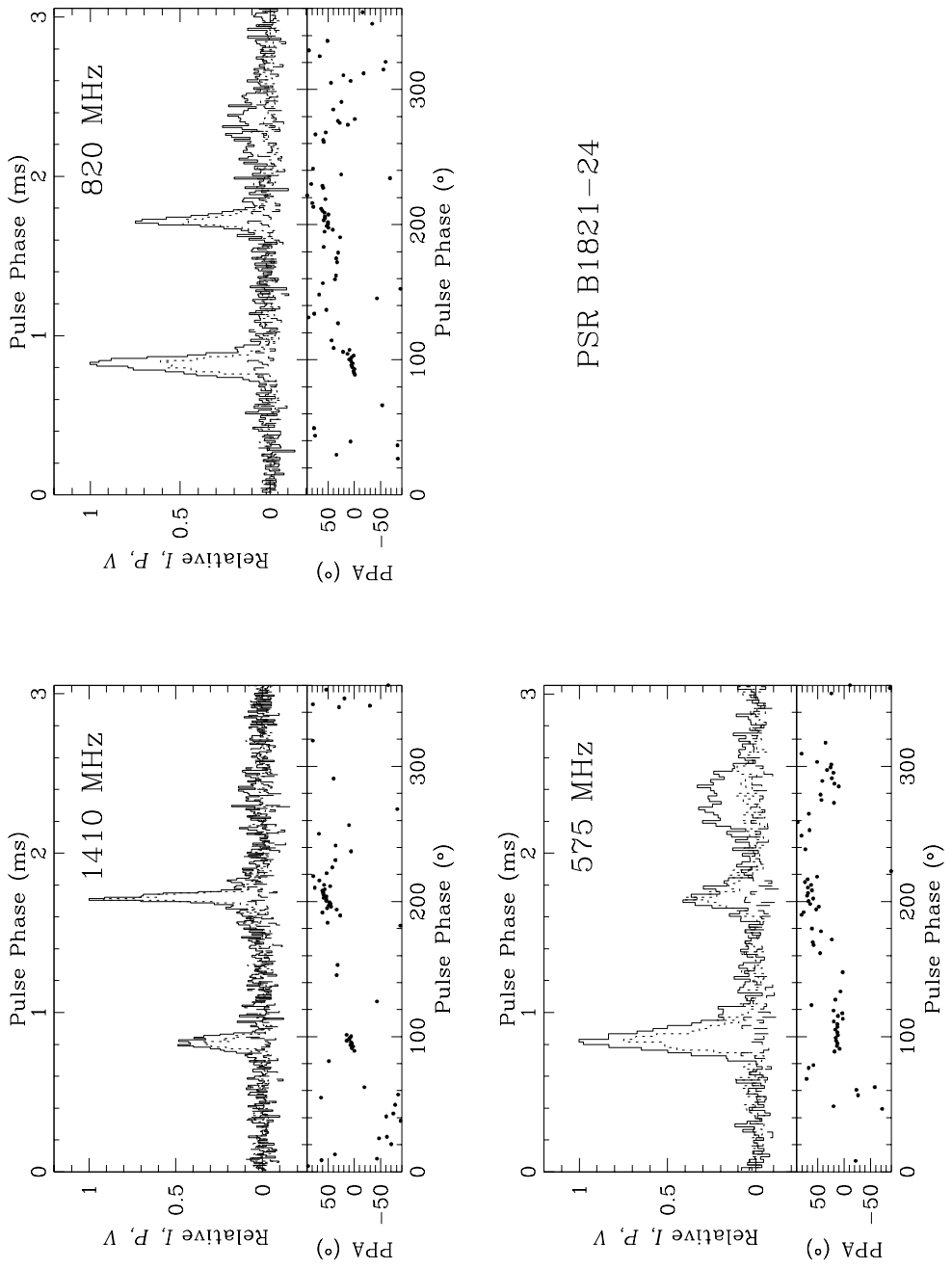


Fig. 3.21.— Polarization profiles of PSR B1821−24 for three radio frequencies. See the caption of Figure 3.2 for details.

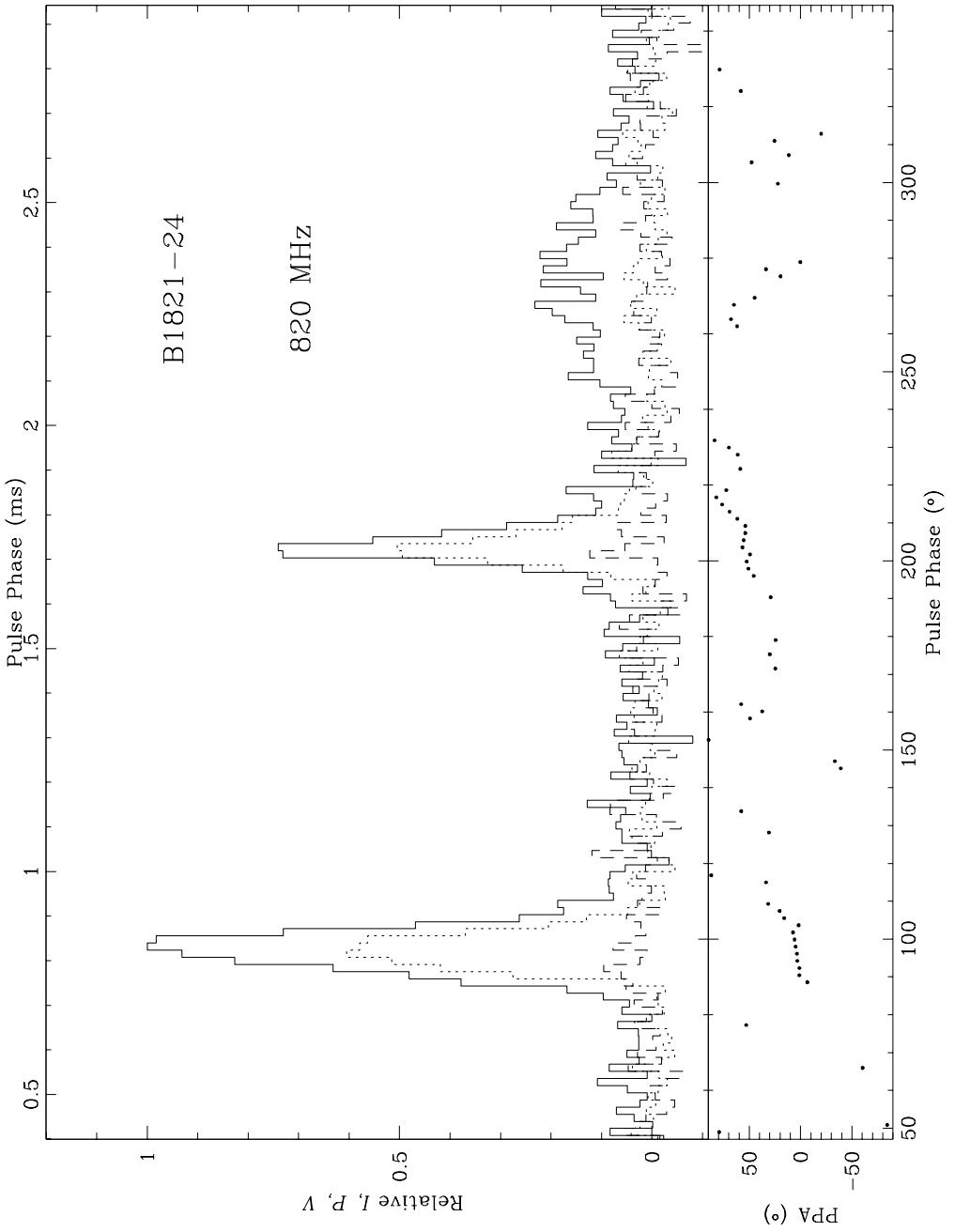


Fig. 3.22.— A region around the pulsed emission has been expanded in the 820-MHz polarization profile of PSR B1821−24. The resolution of this profile is 16.0$\mu$s.

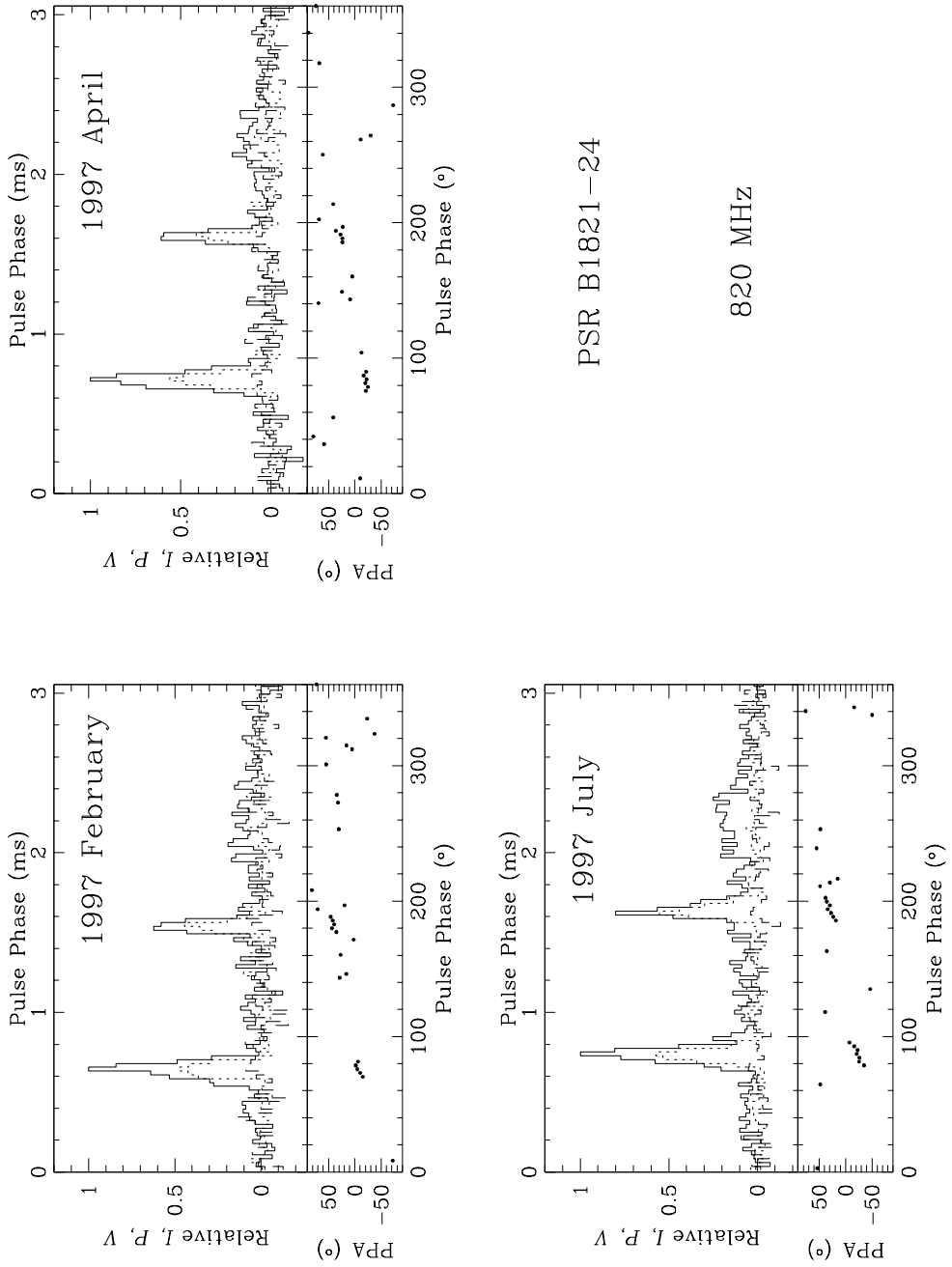


Fig. 3.23.— Polarization profiles of PSR B1821−24 for three epochs at 820 MHz. the caption of Figure 3.2 for details. The second component is stronger relative to the first in 1997 July. Investigation reveals that this amplitude ratio change cannot be explained as a binning effect. The apparent strengthening of the broad component can be explained if the two sharp components are broadened due to increased interstellar scattering.

## 3.9 PSR B1937+21

The fastest millisecond pulsar has a pulse/interpulse morphology at all radio frequencies. The main pulse and interpulse are always separated by $\sim 172°$, in agreement with the observations of Foster, Fairhead & Backer (1991). The effects of interstellar scattering broaden the pulse at low frequencies, hiding these features. These scattering effects are reflected in the 575-MHz component widths for this object listed in Table 3.1. The remaining component widths are comparable to previous measurements (Foster, Fairhead & Backer 1991). Their amplitude ratio remains relatively stable with frequency (cf. Figure 3.25. Both the main pulse and interpulse have trailing secondary features, following a local minimum, at 1410 MHz. These are also visible as shoulders in the 820-MHz profile. These secondary components occur at the pulse phase of the giant pulses which are seen in this pulsar at 430 MHz, and which are discussed in Chapter 6.

The main pulse is relatively strongly polarized, with polarization decreasing from $\sim 60\%$ at 575 MHz to $\sim 30\%$ at 1410 MHz. The interpulse is more weakly polarized. Our results are similar to those reported by Thorsett & Stinebring (1990) at 1420 MHz. Only a small amount of circular polarization is present at any frequency. The polarization position angle remains relatively flat across each pulse, with an orthogonal mode transition on the leading edge of the main pulse at 1410 MHz, the trailing edge of the 820-MHz interpulse, and the leading edge of the 575-MHz interpulse, accompanied by a decrease in the linear polarization.

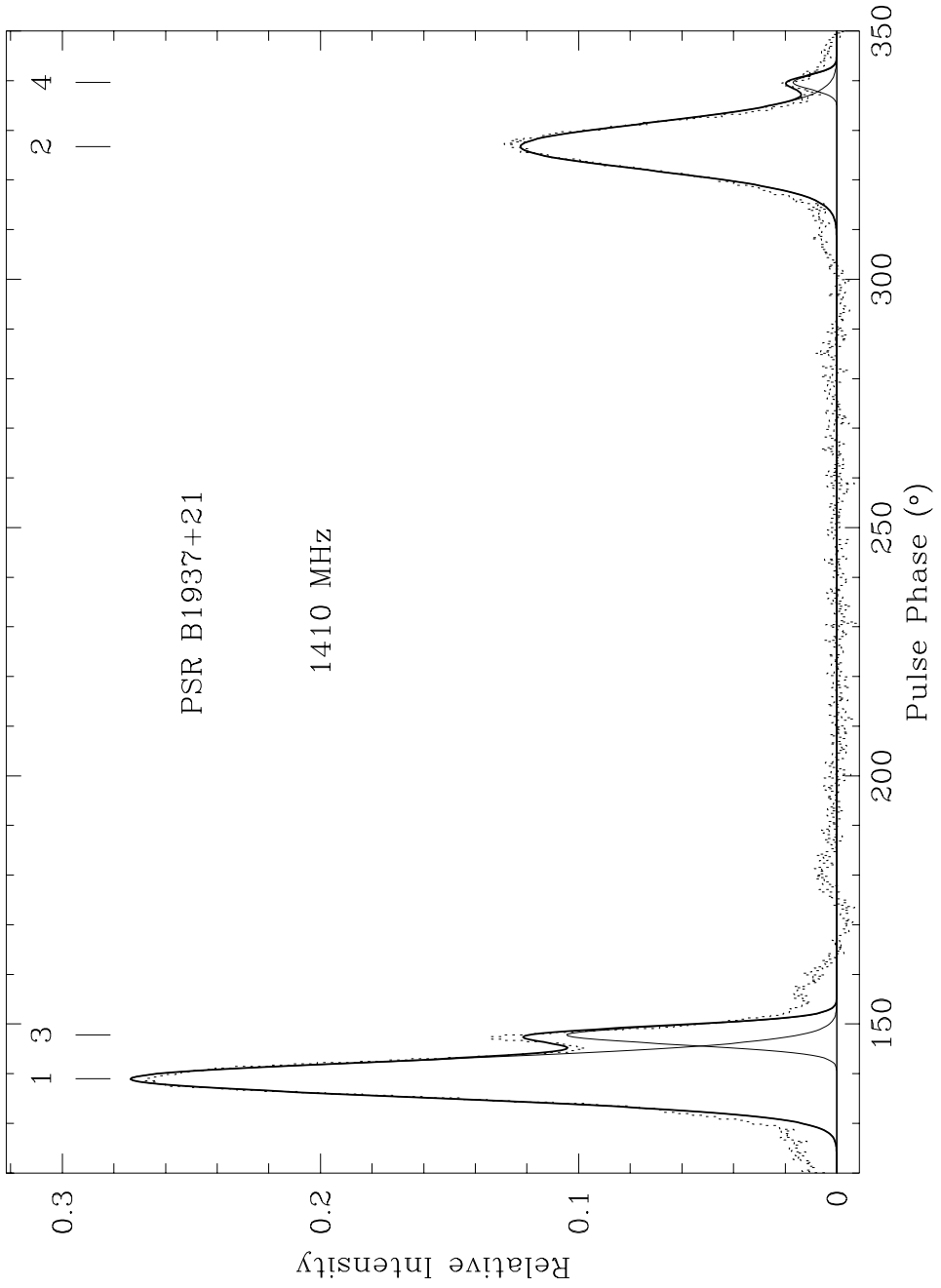


Fig. 3.24.— The Gaussian component decomposition for PSR B1937+21 at 1410 MHz is shown. See the caption of Figure 3.1 for details.

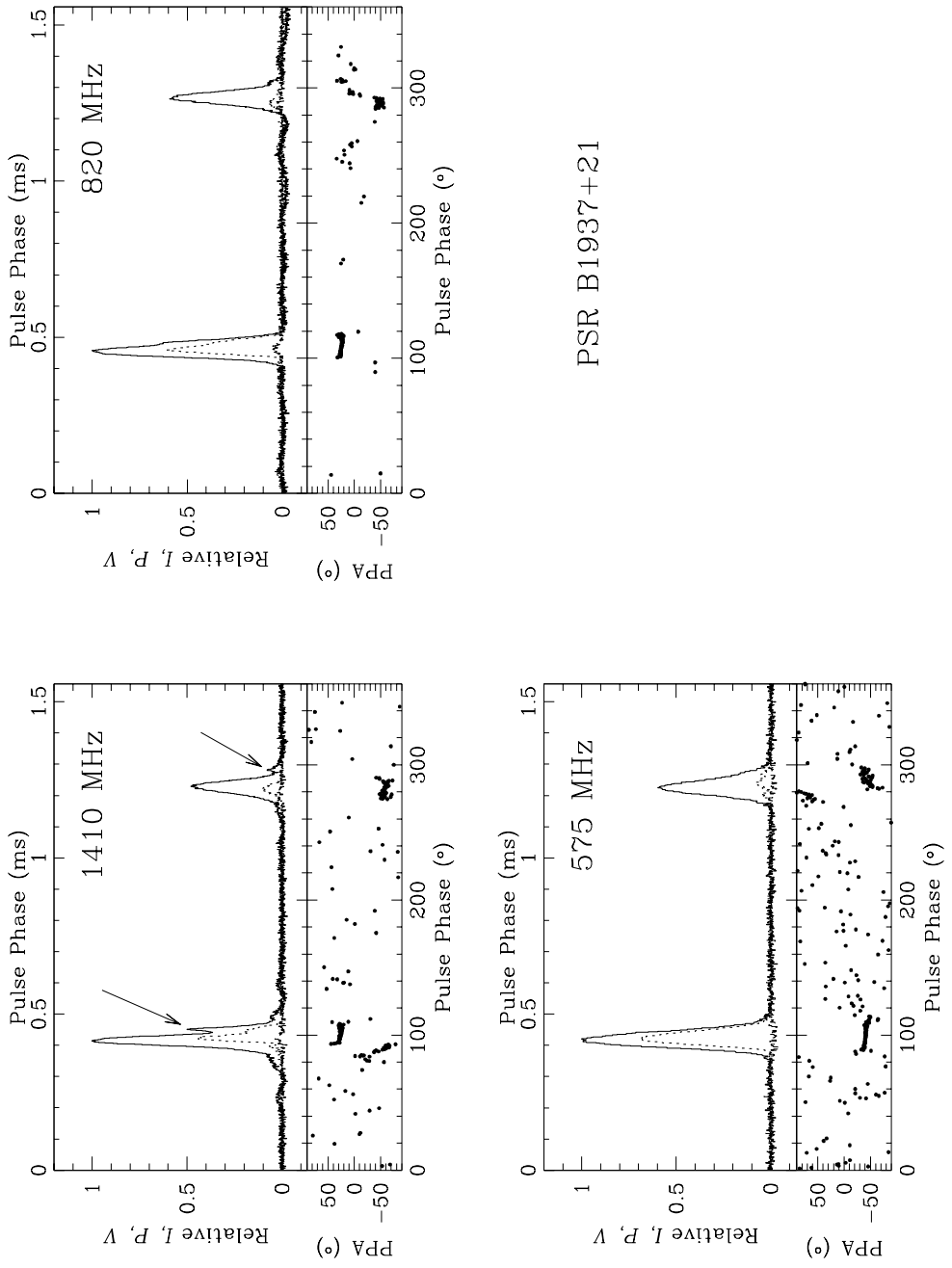


Fig. 3.25.— Polarization profiles of PSR B1937+21 for three radio frequencies. See the caption of Figure 3.2 for details. Systematic variations in the off-pulse baseline at 820 MHz, and at the edges of the pulse at 1410 MHz, are instrumental effects. The arrows point to the secondary maxima, which are at the pulse phase of the 430-MHz giant pulses discussed in Chapter 6.

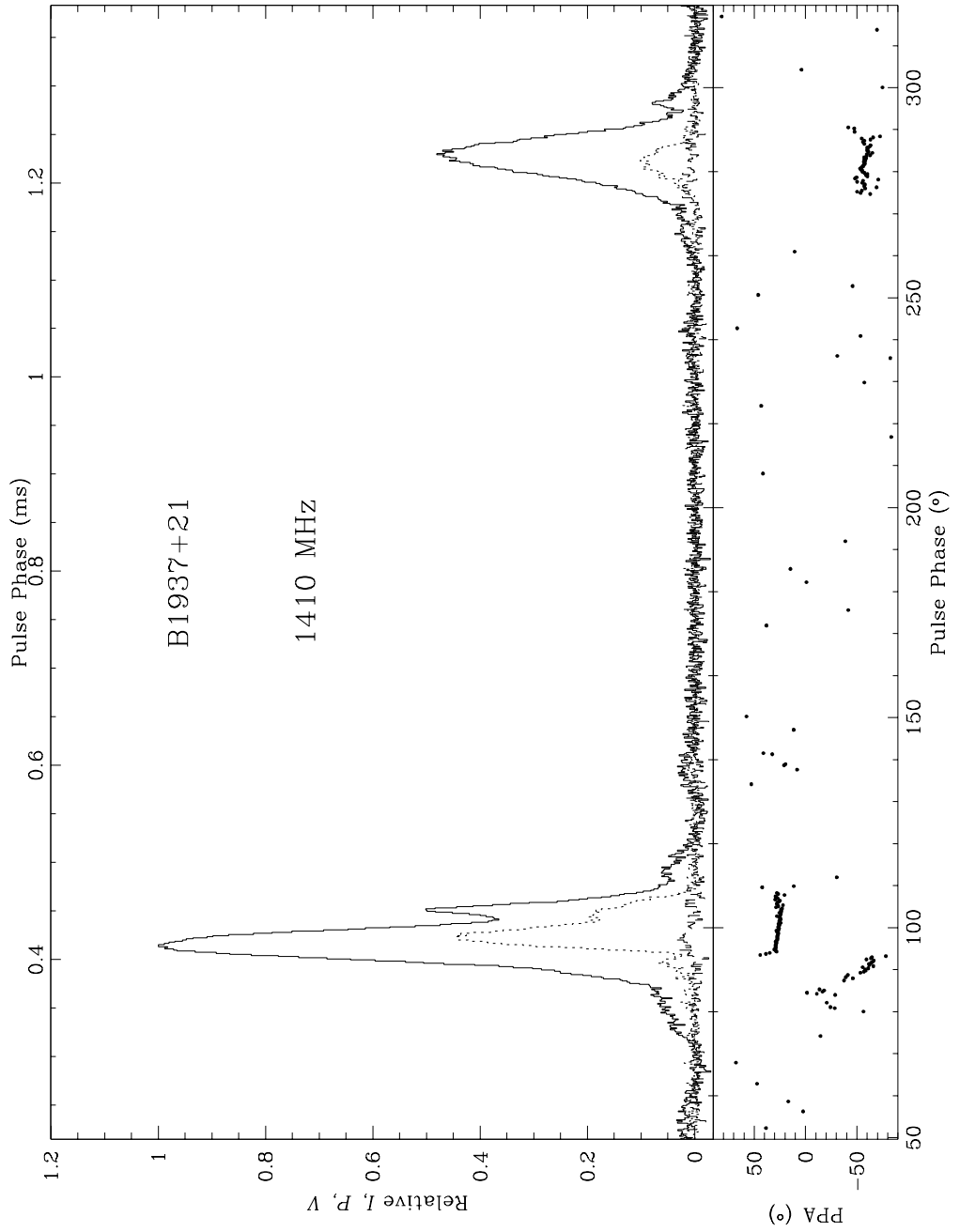


Fig. 3.26.— A region around the pulsed emission has been expanded in the 1410-MHz polarization profile of PSR B1937+21.

## 3.10 PSR J2145−0750

The profile of this 16-millisecond pulsar has been fit with up to 6 components at 1410 MHz (Kramer *et al.* 1998). The main pulse has two main components (1,2), separated by about 70 degrees at all frequencies. A precursor (4) precedes the main peak by 60 degrees, although it is not visible in the 1410-MHz profile shown here. This is consistent with its occasional disappearance in the observations of Xilouris *et al.* (1998). The trailing half of the pulse profile is less important at high frequencies, and is much reduced at 4.85 GHz (Kijak *et al.* 1997). The leading component of the main structure is much less dominant at 100 MHz (Kuzmin & Losovsky 1994). On the basis of published data, Xilouris (1998) concludes that the separation between the precursor and the leading edge of the MP is unchanged between 430, 800, and 1400/1700 MHz, consistent with the results presented here. The data suggest a slight increase in separation of the remaining components with increasing frequency, consistent with that seen by Kuzmin & Losovsky (1994), and contrary to the usual results for normal pulsars. At 1410 MHz, the intensity ratio of the trailing and leading profile components varies in shorter integrations, suggesting moding activity in this pulsar (Xilouris *et al.* 1998). The intensity ratio in our 1410-MHz profile matches that published there. At 820 MHz, the stronger daily averages all have a consistent component ratio, except for a single observation obtained in 1995 February. This profile is displayed in Figure 3.30. The intensity ratio of the two components may vary slightly at 575 MHz, with no significant variation in the accompanying polarization.

The profiles here are only weakly polarized. At 1410 MHz, the first main component is slightly polarized, with linear and circular polarization of order 5-10%, while the rest of the pulse is unpolarized. This same component is again about 10% polarized at 820 MHz and 575 MHz. The strong trailing component is slightly linearly polarized, with depolarization occurring at the orthogonal mode change in the PPA curve. The PPA curve itself is quite complex, but is consistent with frequency. It is most clearly defined in the 820-MHz data, where the displayed profile was accumulated in less than an hour, in a period of extreme amplification due to interstellar scintillation. The orthogonal mode change associated with the trailing portion of the profile is accompanied by reduced linear polarization. A decrease in linear polarization associated with the sharp sweep in PPA under the main pulse suggests that this may be another orthogonal mode transition. The precursor shows significant polarization at these frequencies, and its PPA curve extrapolates to match that of the leading edge of the main pulse. At 820 MHz, the signal is sufficiently strong to determine that the precursor exhibits sense-reversing circular polarization. The

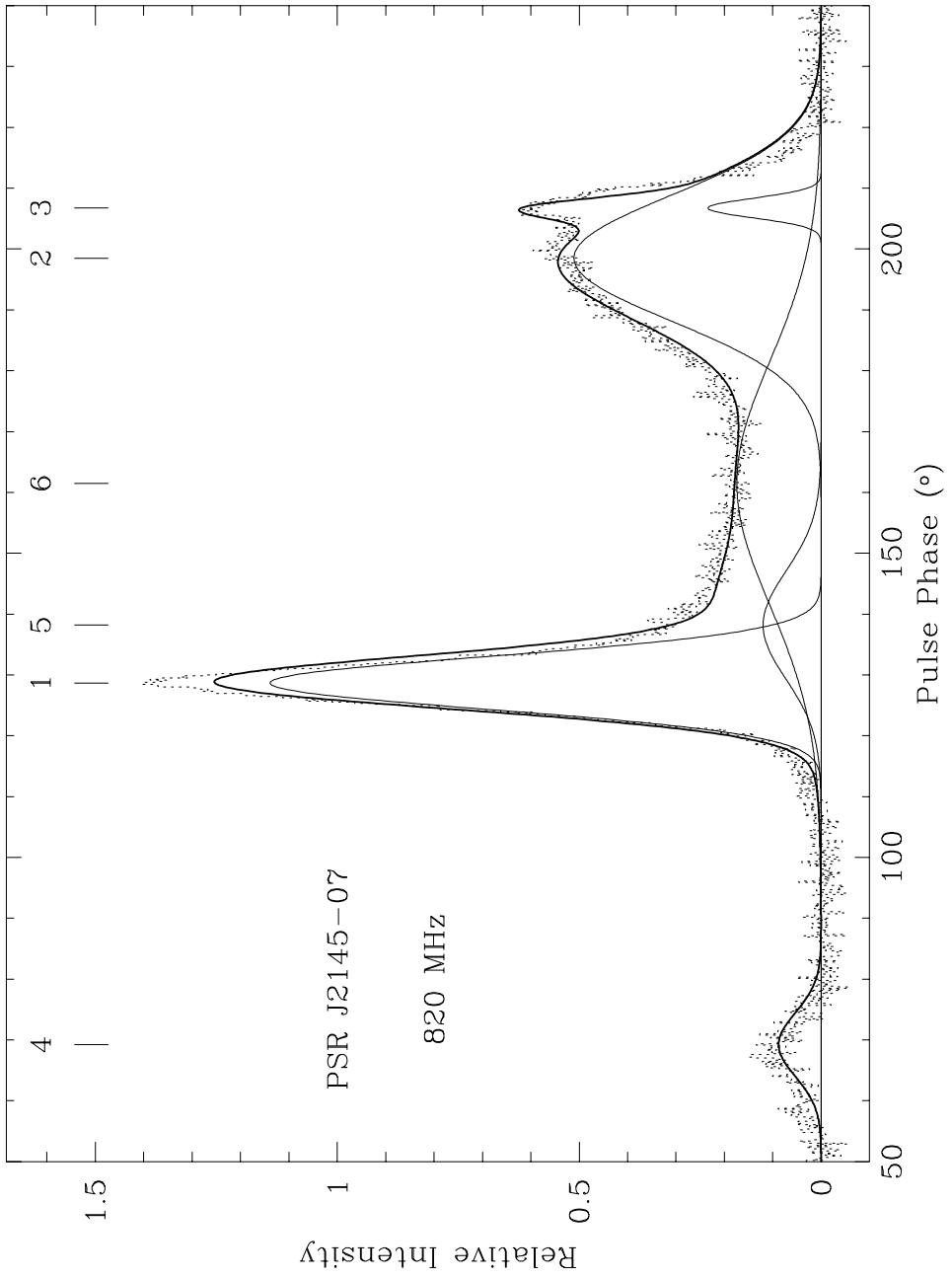


Fig. 3.27.— The Gaussian component decomposition for PSR J2145−0750 at 820 MHz is shown. See the caption of Figure 3.1 for details.

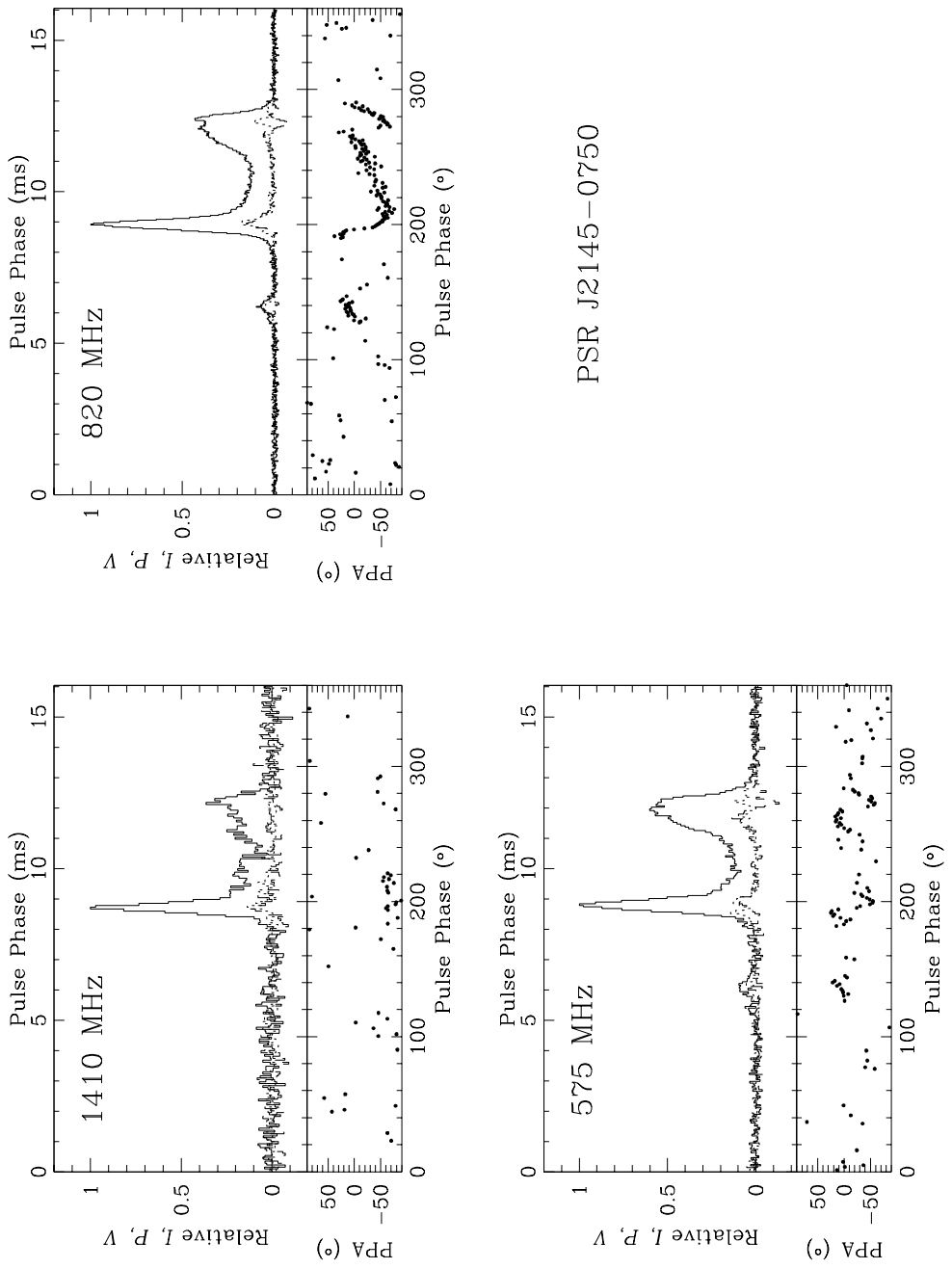


Fig. 3.28.— Polarization profiles of PSR J2145−0750 for three radio frequencies. See the caption of Figure 3.2 for details.

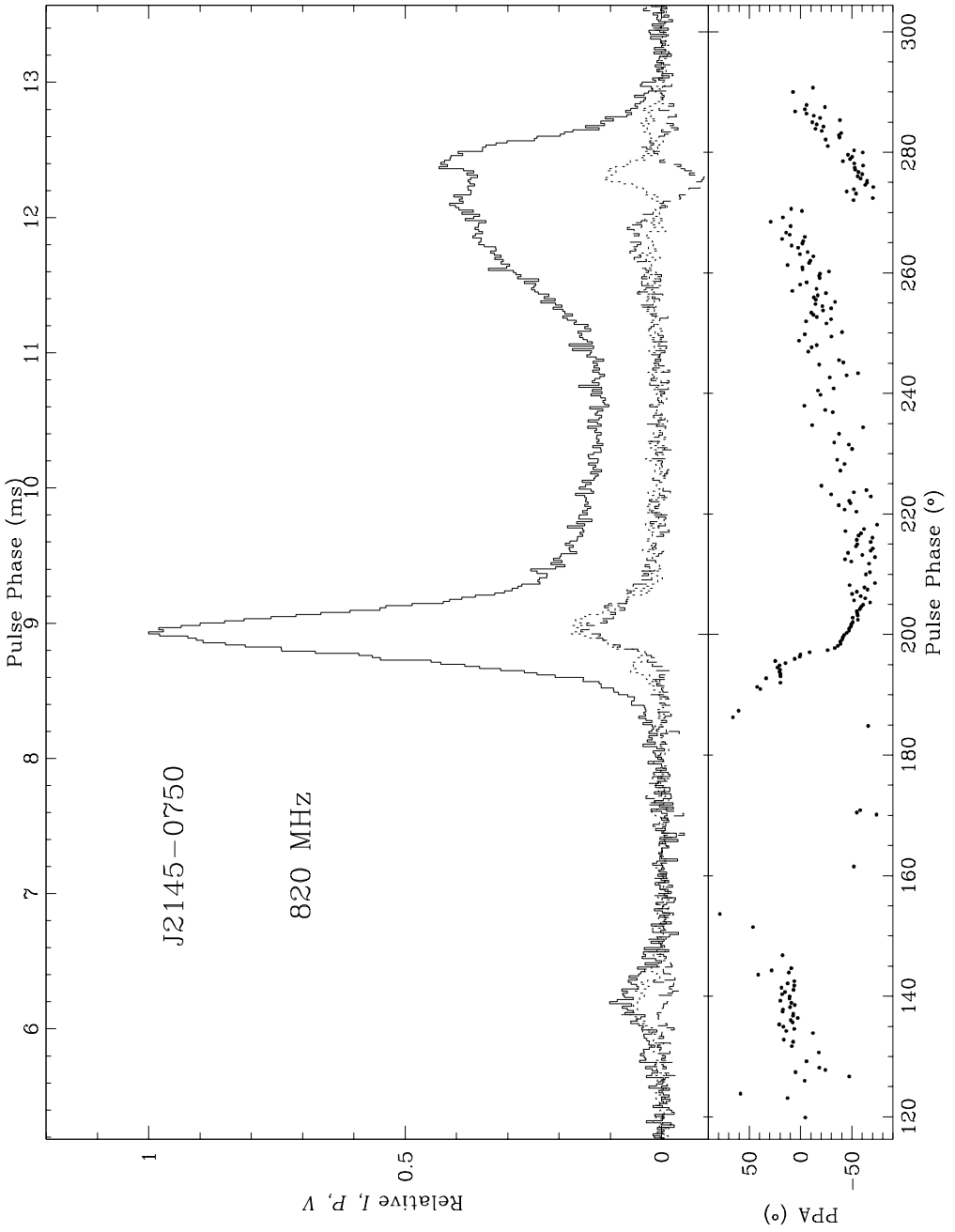


Fig. 3.29.— A region around the pulsed emission has been expanded in the 820-MHz polarization profile of PSR J2145−0750. The resolution of this profile is 16.0 $\mu$s.

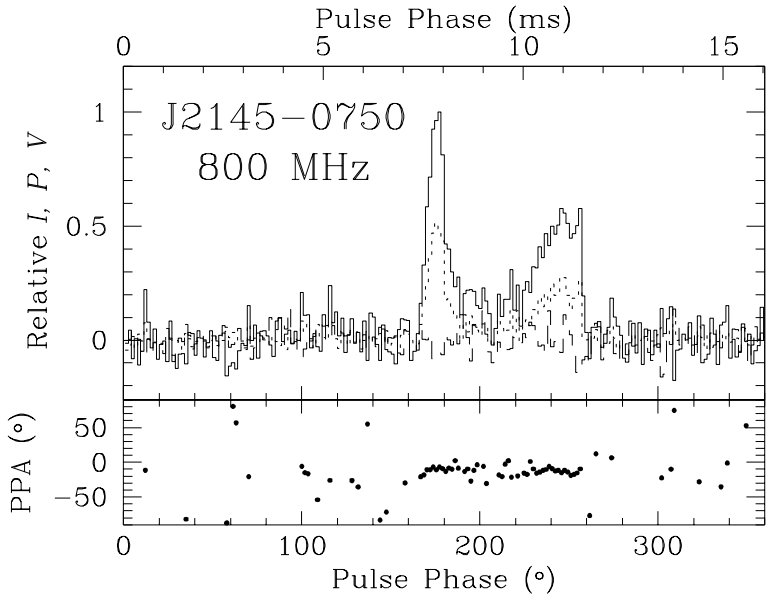


Fig. 3.30.— Polarization profile of PSR J2145−0750 at 800 MHz. This polarization profile resembles that published at 1410 MHz by Xilouris *et al.* (1998). The rest of our data is similar to that in Figure 3.28. The amplitude ratio of the trailing and leading halves of this profile is also different from that seen in the remainder of our data. See the caption of Figure 3.2 for details.

trailing component shows sense-reversing circular polarization of a few percent, while the leading main component is about 10% circularly polarized.

This PPA curve is not like that of Xilouris *et al.* (1998). The published 1410-MHz profile is significantly linearly polarized ($\sim$ 45%), with circular polarization ($-18\%$) mirroring the linear polarization. In two days of observations at widely spaced epochs at 1410 MHz, five days of observations at 575 MHz, and 13 days of observations over four epochs near 800 MHz, only one profile exhibits polarization results similar to the published 1410-MHz data. That 800-MHz profile, obtained in 1995 February, is precisely the one for which a different intensity ratio between the two main components was found (cf. Figure 3.30). This suggests that the intensity and polarization moding are related. Although the circular polarization is still weak, the linear polarization is about 50% and the PPA curve is extremely flat. Other profiles obtained in the same observing epoch are similar to that displayed in Figure 3.28. For this pulsar, not only does the polarized fraction vary, but the PPA curve undergoes a radical transformation at the same time.

## 3.11 1410-MHz Polarization Profiles

Polarization profiles were obtained for several pulsars at 1410 MHz, for which no usable information was obtained at other radio frequencies. These are presented in Figures 3.31-3.32 for completeness.

### 3.11.1 PSR J0751+1807

The profile of this pulsar is relatively symmetric at 1410 MHz. The polarization results are similar to those presented by Xilouris *et al.* (1998), who found that the linearly polarized fraction of the leading component fluctuated, along with its associated PPA. The profile shape, and polarization properties of the trailing component remained stable.

### 3.11.2 PSR 1518+4904

This double-peaked profile has a post-cursor which follows the main pulse by about 25° (Kramer *et al.* 1998). Although the linear and circular polarized fractions are similar, the polarization properties displayed here do not match those of Xilouris *et al.* (1998). The linear polarization is significant here only in the leading portion of the pulse, as opposed to the trailing edge of the profile in that work. The SNR of this profile is too weak to meaningfully compare the PPA results.

### 3.11.3 PSR 1640+2224

Only a small amount of polarization is present here, whereas Xilouris *et al.* (1998) present a highly polarized profile, with no mention of variations.

### 3.11.4 PSR 1643−1224

This profile is once again much less polarized than the profile presented by Xilouris *et al.* (1998), although the PPAs are similar. An orthogonal mode is apparently present near the center of the pulse, accompanied by linear depolarization, and a reversal in the sense of the weak circular polarization. This, along with the pulse morphology, suggests that this is a core component with conal outriders.

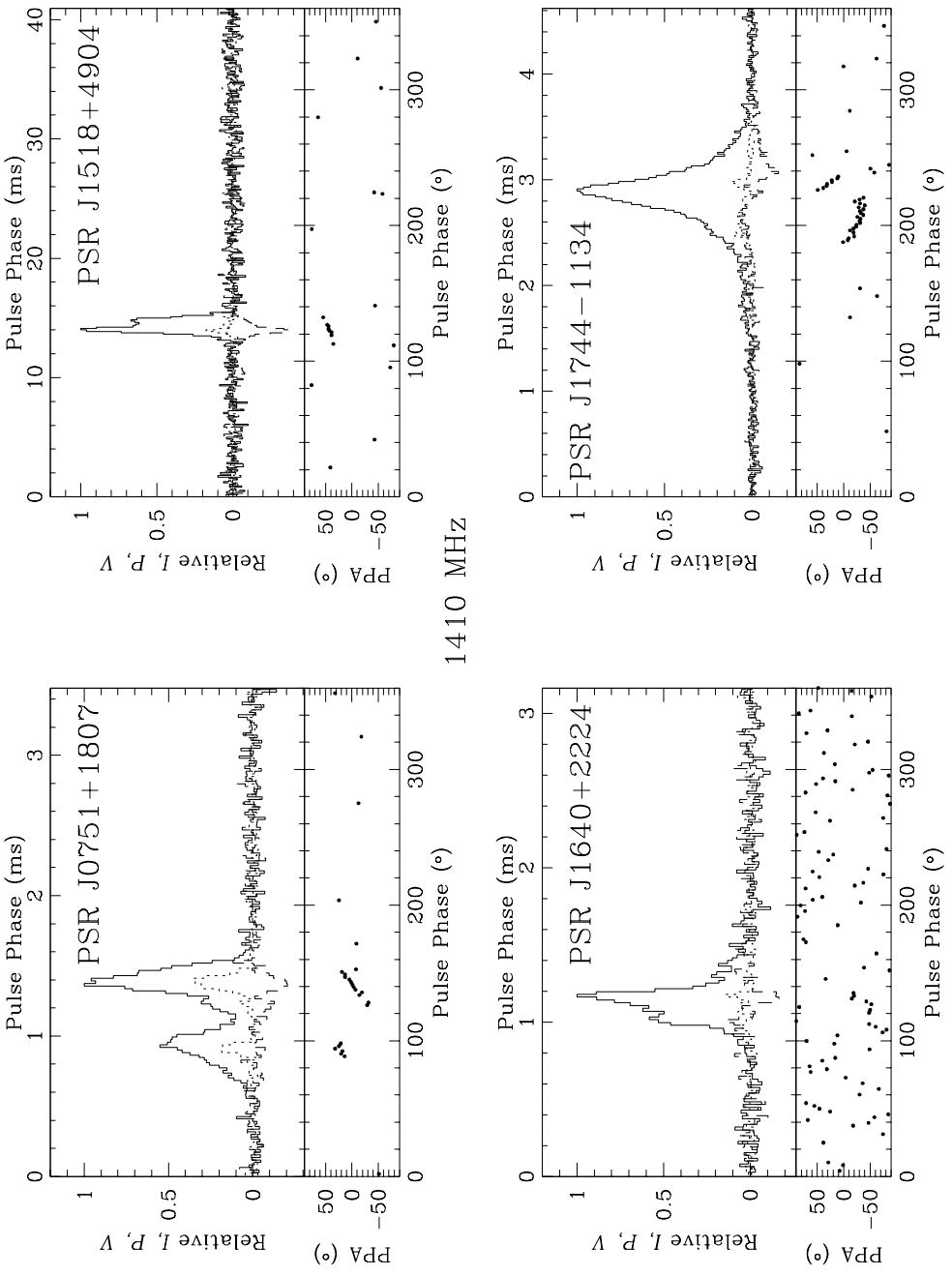


Fig. 3.31.— Polarization profiles of PSRs J0751+1807, J1518+4904, J1640+2224 , and J1643−1224at 1410 MHz. See caption of Figure 3.2 for details.

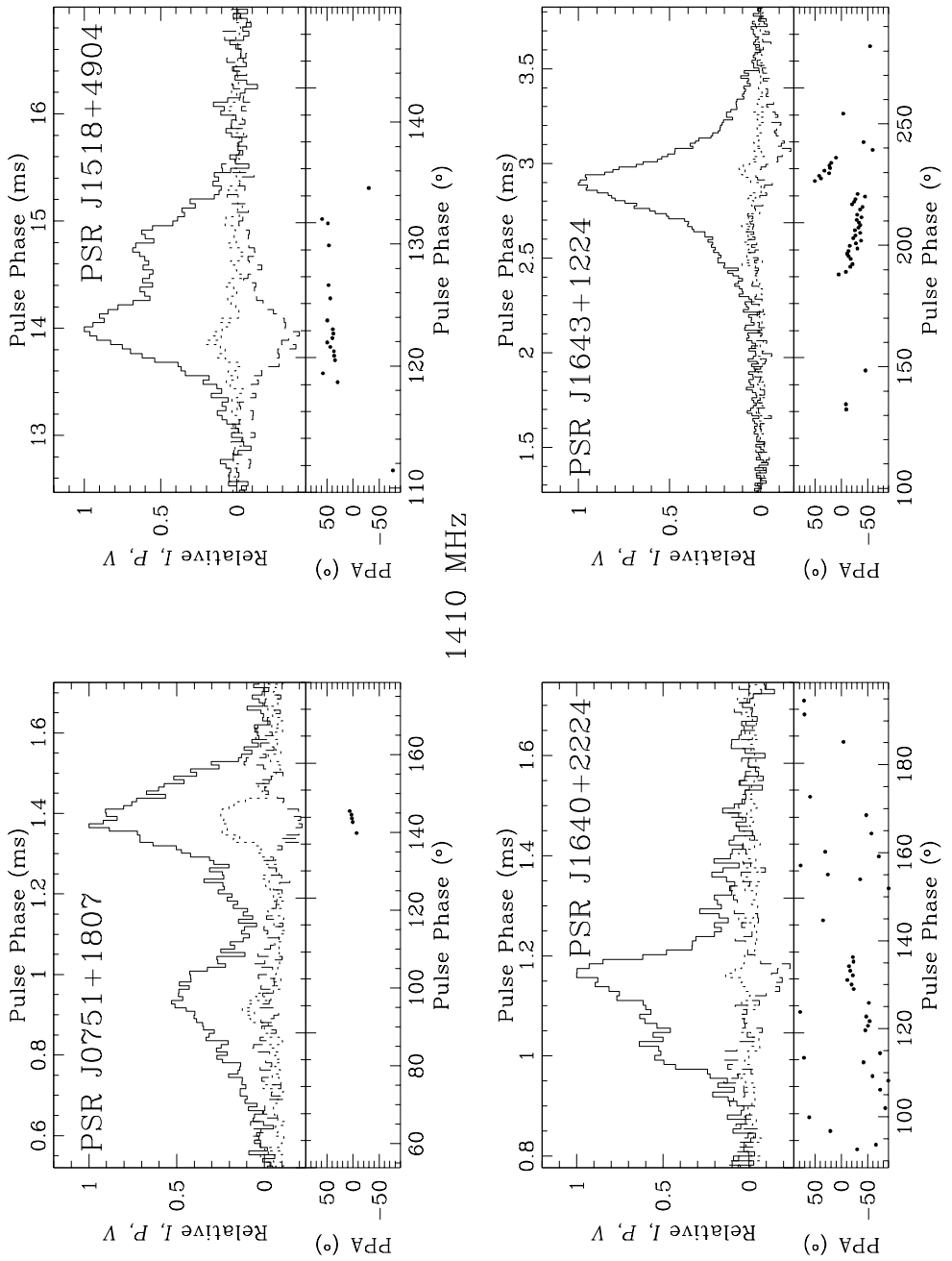


Fig. 3.32.— A region surrounding the pulsed emission has been expanded for the polarization profiles of PSRs J0751+1807, J1518+4904, J1640+2224 , and J1643−1224at 1410 MHz. See caption of Figure 3.2 for details. The resolutions of the four profiles are 9.1 $\mu$s, 41.1$\mu$s, 13.7 $\mu$s and 9.1 $\mu$s.

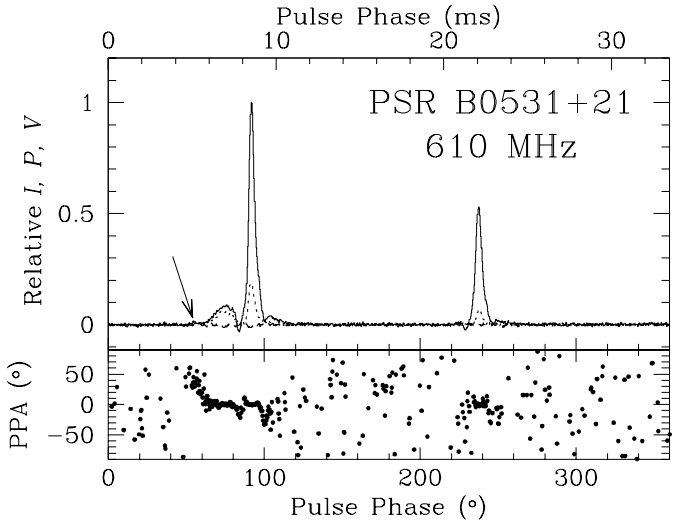


Fig. 3.33.— A polarization profile of PSR B0531+21 at 610 MHz is displayed for 34.75 hours of data. The the relative intensity, linear, and circular polarizations are plotted against pulse phase using solid, dotted, and dashed lines, respectively. The bottom axis indicates the pulse phase in degrees, while the top axis displays the same quantity in milliseconds. The polarization position angle (PPA) is plotted for phases where the linear polarization exceeds the off-pulse *rms*. The resolution of the plot is 34.1 $\mu$s. The arrow points to the position of the low frequency component (LFC) detected by Moffett & Hankins (1996).

## 3.12 PSR B0531+21 at 610 MHz

The 610-MHz high resolution profile of the Crab pulsar shown in Figure 3.33 is consistent with multifrequency profiles from Moffett & Hankins (1996). These data show the presence of the low frequency component (LFC) which they see above 600 MHz, just before the precursor. The polarization profile indicates that the precursor is highly polarized, while the main pulse (MP) and interpulse (IP) are $\sim$ 20% polarized. No significant circular polarization is seen. The position angle curve has a series of relatively flat (slightly downward) trends across each of the three largest components. The excursions from a slow linear trend in the MP and IP are due to artifacts in the profile are caused by the GBPP's use of a dedispersion filter with a slightly incorrect length. Note that the LFC has a much sharper trend in position angle. The MP, IP, and precursor properties are similar at lower frequencies (Campbell, Heiles & Rankin 1970, Manchester 1971, Manchester, Huguenin & Taylor 1972). At frequencies above 1400 MHz, the precursor is no longer visible, but the main pulse and interpulse polarization properties remain similar to those shown here (Manchester 1971, Moffett 1997). Moffett (1997) finds that at 1400 MHz, the LFC is about 40% polarized, and the main pulse shows weak sense-reversing circular polarization. The PPA is similar

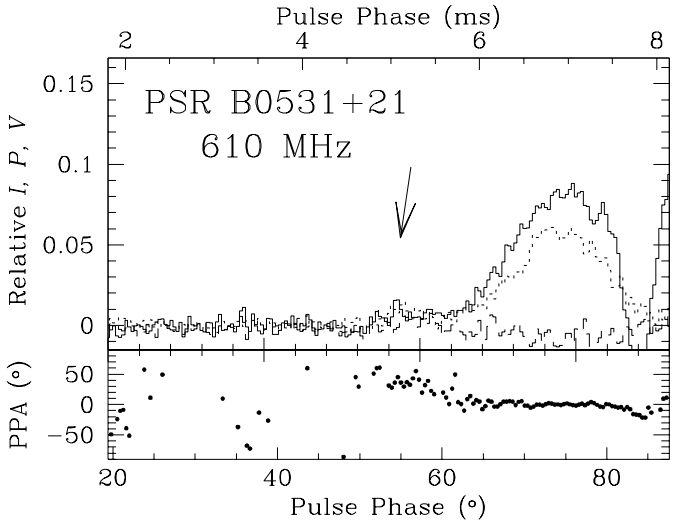


Fig. 3.34.— The region near the LFC and precursor are expanded in this plot of the 610-MHz polarization profile of PSR B0531+21.

to that displayed here. At still higher frequencies, the pulse morphology changes dramatically (Moffett 1997).